Patient-derived microphysiological model identifies the therapeutic potential of metformin for thoracic aortic aneurysm

Wenrui Ma,[a,1] Jingjing Zhang,[a,b,1] Shaowen Liu,[a] Shiqiang Yan,[a] Kehua Xu,[a] Yu Shrike Zhang,[c] Mieradilijiang Abudupataer,[a] Yang Ming,[a] Shichao Zhu,[a] Bitao Xiang,[a] Xiaonan Zhou,[a] Shaman Luo,[a,b] Hui Huang,[a] Yuyi Tang,[d] Shan Zhang,[a] Zhuxin Xie,[a] Nan Chen,[a] Xiaoning Sun,[a] Jun Li,[a] Hao Lai,[a] Chunsheng Wang,[a]* Kai Zhu,[a]* and Weijia Zhang [a,b,e]*

[a]Department of Cardiac Surgery, Zhongshan Hospital Fudan University, Institutes of Biomedical Sciences, Shanghai Institute of Infectious Disease and Biosecurity, Shanghai Medical College, Fudan University, Shanghai 200032, China
[b]The State Key Laboratory of Molecular Engineering of Polymers, Fudan University, Shanghai 200438, China
[c]Division of Engineering in Medicine, Department of Medicine, Brigham and Women's Hospital, Harvard Medical School, Cambridge, Massachusetts 02139, United States
[d]Cardiovascular Research Laboratory, Shanghai Fifth People's Hospital, Fudan University, Shanghai 200240, China
[e]The Shanghai Key Laboratory of Medical Imaging Computing and Computer Assisted Intervention, Shanghai Medical College of Fudan University, Shanghai 200433, China

eBioMedicine 2022;81: 104080
Published online xxx
https://doi.org/10.1016/j.ebiom.2022.104080

Summary

Background Thoracic aortic aneurysm (TAA) is the permanent dilation of the thoracic aortic wall that predisposes patients to lethal events such as aortic dissection or rupture, for which effective medical therapy remains scarce. Human-relevant microphysiological models serve as a promising tool in drug screening and discovery.

Methods We developed a dynamic, rhythmically stretching, three-dimensional microphysiological model. Using patient-derived human aortic smooth muscle cells (HAoSMCs), we tested the biological features of the model and compared them with native aortic tissues. Drug testing was performed on the individualized TAA models, and the potentially effective drug was further tested using β-aminopropionitrile-treated mice and retrospective clinical data.

Findings The HAoSMCs on the model recapitulated the expressions of many TAA-related genes in tissue. Phenotypic switching and mitochondrial dysfunction, two disease hallmarks of TAA, were highlighted on the microphysiological model: the TAA-derived HAoSMCs exhibited lower alpha-smooth muscle actin expression, lower mitochondrial membrane potential, lower oxygen consumption rate and higher superoxide accumulation than control cells, while these differences were not evidently reflected in two-dimensional culture flasks. Model-based drug testing demonstrated that metformin partially recovered contractile phenotype and mitochondrial function in TAA patients' cells. Mouse experiment and clinical investigations also demonstrated better preserved aortic microstructure, higher nicotinamide adenine dinucleotide level and lower aortic diameter with metformin treatment.

Interpretation These findings support the application of this human-relevant microphysiological model in studying personalized disease characteristics and facilitating drug discovery for TAA. Metformin may regulate contractile phenotypes and metabolic dysfunctions in diseased HAoSMCs and limit aortic dilation.

Funding This work was supported by grants from National Key R&D Program of China (2018YFC1005002), National Natural Science Foundation of China (82070482, 81771971, 81772007, 51927805, and 21734003), the Science and Technology Commission of Shanghai Municipality (20ZR1411700, 18ZR1407000, 17JC1400200, and 20YF1406900), Shanghai Municipal Science and Technology Major Project (2017SHZDZX01), and Shanghai Municipal Education Commission (Innovation Program 2017-01-07-00-07-E00027). Y.S.Z. was not supported by any of these funds; instead, the Brigham Research Institute is acknowledged.

Keywords: Microphysiological model; Organ on a chip; Vascular smooth muscle cell; Aortic aneurysm; Mitochondrial dysfunction; Metformin

*Corresponding authors.
E-mail addresses: wangchunsheng@fudan.edu.cn (C. Wang), zhu.kai1@zs-hospital.sh.cn (K. Zhu), weijiazhang@fudan.edu.cn (W. Zhang).

[1] Contributed equally to this study.

Research in context

Evidence before this study

Thoracic aortic aneurysm (TAA) is a silent yet lethal disease with few effective medications. The interspecies difference and nonrepresentative pathogenesis in the animal disease models have led to frequent failures in clinical trials. Human-relevant microphysiological devices can be advantageous in modeling diseases, which have shown promising results in predicting patients' responses to medical treatment. Previous cohort studies have shown that metformin may be associated with a reduced risk of abdominal aortic aneurysm.

Added value of this study

We develop a patient-derived microphysiological model reflecting the hallmarks of TAA tissues, which recapitulates phenotypic switching and mitochondrial dysregulation in the diseased aortic smooth muscle cells. Model-based drug testing shows the possibility of metformin in recovering cellular phenotype and mitochondrial function. Mouse TAA model and human clinical data validate that metformin may maintain contractile phenotype and delay aortic dilation.

Implications of all the available evidence

Our study supports the use of microphysiological models in drug screening for aortic diseases and proposes mitochondrial boosters such as metformin as potential therapeutic options for TAA.

Introduction

Thoracic aortic aneurysm (TAA) is a common aortic disease characterized by local or diffuse dilation of the thoracic aortic wall, the most load-bearing part of the human aorta.[1-3] Based on Laplace's law, the increase in thoracic aortic diameter and decrease in mural thickness leads to elevated tension in the aortic wall[4]. Once a certain threshold is reached, the diseased aortic wall may collapse and develop into acute aortic dissection or rupture, causing extremely high mortality (dissection, 20%–75%; rupture, 80%–100%).[1] Apart from the inheritable connective tissue disorders such as Marfan syndrome, most patients diagnosed with TAA are sporadic cases that do not have a clear genetic causality.[5-7] Whilst surgical repair remains to be the standard treatment of TAA, the operational risks have encouraged researchers to discover medications capable of controlling TAA, *i.e.*, delaying increase in thoracic aortic diameter and reducing risks of lethal aortic events.[8,9] However, discovery of drugs for aortic aneurysm has been considerably hampered: the interspecies difference and nonrepresentative pathogenesis in the current animal models have led to frequent failures in clinical trials.[9,10]

An important methodology of human-relevant *in vitro* disease modeling is the microphysiological platform that is developed to emulate the physiological microenvironment of tissues or organs.[11-15] As minimalist yet controllable microsystems, such models can replicate the biomechanical stimuli affecting cells residing in tissues.[16-18] Recently, multiple three-dimensional (3D) culture substrates, including hydrogels and protein mixtures, have been modified in the development of microphysiological models.[19] Gelatin methacryloyl (GelMA) is a nature-derived, photocrosslinkable biomaterial that can form hydrogels with tunable stiffness and good biocompatibility, which has been widely used as a biomimetic extracellular matrix in bioprinting, tissue engineering, and drug delivery.[11,20-24] The GelMA-based hydrogels have also been utilized in constructing heart-on-a-chip and vessel-on-a-chip models.[25,26]

In cardiac cycles, human aortic smooth muscle cells (HAoSMCs) in the thoracic aorta receive rhythmic tensile strain, which plays a key role in regulating cellular behavior and maintaining biological homeostasis.[27-29] Notably, HAoSMCs cultured in a two-dimensional (2D) static environment exhibited phenotypic switching from a contractile to a synthetic phenotype, which does not reflect a physiological state but rather a well-reported pathological condition related to aneurysmal formation.[30-32] There is also accumulating evidence that mitochondrial function may be implicated in the development of TAA.[33,34] It was postulated that impaired mitochondrial respiration might cause insufficient ATP production for contractile activities, which has not been assessed in HAoSMCs cultured *in vitro*[35]. Hopefully, a 3D, dynamic, HAoSMC-based microphysiological model may recapitulate the pathophysiological features and provide more accurate assessment of drug response in patients with TAA. Previous studies have developed multiple 3D dynamic devices for studying the effect of biomechanical stimuli on vascular smooth muscle cells.[36-39] These studies focused on how cellular phenotype changed in response to biomechanical factors, but few attempted to emulate the biological characteristics of the healthy and diseased vascular tissue, or to perform multiple drug testing on patient-derived individualized aortic models as in tumor-on-a-chip models.[40]

Here, we report the development of an aortic microphysiological model that emulates the pathophysiology of TAA. In this model, primary HAoSMCs were encapsulated in a 3D hydrogel with rhythmic tensile strain, mimicking the dynamic expansion and relaxation of the aorta. Expressions of the disease-related genes were analyzed to validate the aortic emulation of the model. Contractile phenotype and mitochondrial function were compared between 3D and 2D models. Three drugs with potential effects on aortic homeostasis were tested on the personalized TAA models.[41-45] Finally, mouse experiments and institutional clinical study were

performed to validate the results of the microphysiological model-based drug testing.

Methods

GelMA synthesis and hydrogel preparation

GelMA hydrogels were produced and characterized as described previously.[46] Briefly, type A gelatin (G1890, Sigma-Aldrich) was dissolved in phosphate-buffered saline (PBS, Gibco) at a concentration of 10% (w/v). The mixture was stirred with a magnetic stir bar at 55°C for 30 minutes to 1 hour until its complete dissolution. Stirring was intensified when methacrylic anhydride (276685, Sigma-Aldrich) was added into the dissolved gelatin (0.6:1, v/v). Stirring was continued for up to 3 hours until the solution turns homogeneously opaque. The solution was diluted with PBS, transferred into dialysis bags, and dialyzed at 50°C against a large volume of sterile filtered deionized water for 7 days until the GelMA solution was clear and the pungent odor disappeared. Subsequently, GelMA was titrated to pH 7.4, filtered using 0.22-μm syringe filters, lyophilized, and stored at 4°C. The degree of functionalization (DoF) was tested for each batch of GelMA using the ninhydrin assay technique (3 batches: DoF = 76.1±4.0%). For cell culture and encapsulation, the GelMA precursor solution was prepared at 10% (w/v) with photoinitiator Irgacure2959 (H1361, TCI) at concentrations of 0.25% (w/v) in PBS.

Model design, fabrication, and assembly

The microphysiological model was composed of two polydimethylsiloxane (PDMS; RTV615, Momentive) slabs polymerized in defined casts at a 10:1 weight ratio of base to curing agent at 70°C for 1 hour. Master molds were fabricated using standard laser cutting on acrylic plates. The PDMS slabs were peeled off the molds. Before bonding, the top layer was finalized by punching circular access ports with 1-mm microfluidic punchers for inlets and outlets of culture medium and GelMA-cell mixture. Subsequently, the opposing surfaces of both layers were treated with air plasma (Harrick Plasma) and 30 minutes of incubation at 70°C to achieve stable bonding. Afterwards, polydopamine coating was performed to reinforce hydrogel adhesion to the PDMS model.[47] Briefly, the culture surfaces of the bottom layer were incubated with 2 mg/ml of dopamine solution (H8502, Sigma-Aldrich) prepared in 10-mM Tris-HCl (titrated to pH 8.5; T105287, Aladdin) for 24 hours at room temperature, which was injected into the assembled models from the GelMA inlets. After incubation, the polydopamine solution was gently aspirated, and the PDMS surfaces were washed twice with sterile filtered deionized water to remove unbound dopamine molecules. The tubes were inserted into the inlets and outlets for culture medium, and the joints were sealed using PDMS to avoid medium leaking. The models were further heated at 70°C for 30 minutes, stored at room temperature, and sterilized under ultraviolet light for 2 hours before use. A set of microelectromechanical apparatus was used to deliver rhythmic, uniaxial tensile strain to the PDMS model and the GelMA hydrogel on the model. A stepper motor, controlled by a computer numerical control apparatus, was used to generate tensile strain with confined frequency and magnitude.

Finite element analysis

The aim of the finite element analysis was to evaluate: 1) whether the tensile strain in the hydrogel reached the desired strain level, and 2) whether the untoward strain outliers were significant. Computations were performed using ANSYS 16.0 (ANSYS Inc.). A total of 6 pillar combinations, in which cubic and cylindrical pillars arrayed in 2 × 4, 3 × 5, and 3 × 6 fashions, were simulated in the setting of a 10% elongation of the culture pool in the strain direction. Both the pillars and the hydrogel were meshed using a total of 48,508 eight-node hexahedral elements. Perfect lubrication was considered in the contact between the hydrogel and the pillars and between the hydrogel and the walls of the culture pool, and the hydrogel was considered tightly fixed to the bottom of the culture pool. The interactions between the PDMS pillars and the hydrogel were modeled using a surface-to-surface contact. The Young's modulus and Poisson ratio of PDMS were set to 2.61 MPa and 0.5, respectively, as reported previously.[48] The GelMA-based hydrogel's modulus was set to 8.67 kPa, based on our measurement on Day 14 under static incubation. The Poisson ratio was set to 0.33 for the hydrogel.[16]

Confined strain validation

The strain field was assessed experimentally along the short and long axes of the culture pool. The GelMA hydrogel was prepared as previously indicated, with carbon fiber powder (average length: 48 μm) fully mixed and encapsulated. Images of the powder particles were acquired at the static and the 10% strain phases using an optical microscope (DMi8, Leica). For each sample, three sites of the hydrogel were considered. For each site, 5 pairs of powder particles at different heights within the hydrogel were considered, and for each pair the mutual distance was measured along the short and long axes before and after stretching. Strain of the two directions was calculated as $(\text{distance}_{\text{strain}} - \text{distance}_{\text{static}}) / \text{distance}_{\text{static}} \times 100\%$. The measured strain was used to compare with the computational simulations.

Human aortic tissue fragment collection and cell isolation and expansion

The human ascending aortic tissues were obtained from 4 patients who underwent cardiac surgery with normally

functioning tricuspid aortic valve and non-diseased ascending aorta, and from 8 patients with nonhereditary, sporadic TAA who underwent ascending aorta replacement, after informed consent from relatives and in accordance with the local ethics committee (Zhongshan Hospital Fudan University Ethics Committee Approval Letter No. B2020-158R; Supplemental Table 1). The normal and diseased aortic specimens were immediately transferred to the laboratory in cold PBS, which were cut into 2 halves for tissue experiments and harvest of HAoSMCs. Primary HAoSMCs were successfully expanded from 3 patients with normal aortas (1 female aged 38, 1 male aged 22, and 1 male aged 31) and from all 8 patients with TAA. The intima and adventitia layers were carefully removed, and the media layer was minced into 2 mm × 2 mm pieces and allowed to adhere to the culture flasks. Smooth muscle cell medium (1101, ScienCell Research) was added when adherence was stable. After approximately 3 weeks, when cells were about 80% confluent, the cells were passaged using 0.25% trypsin/ethylenediaminetetraacetic acid and re-plated.

Construction of human microphysiological model

The control microphysiological model was generated by embedding the nondiseased HAoSMCs into a crosslinkable GelMA-based hydrogel matrix into the device. The cell-laden GelMA prepolymer solution at a cell density of 10^6 cells/ml was injected into the culture channel of the device (approximately 700 μl/device), and was immediately crosslinked by UV light (800 mW/cm^2) for 60 seconds before filling the upper channel with Dulbecco's modified Eagle's medium (DMEM, Gibco) containing 10% fetal bovine serum (Gibco) and 1% penicillin-streptomycin (Gibco). Culture medium was changed at 15 minutes, 30 minutes and 1 hour after gelation to wash off ungelated polymers. The 3D HAoSMC-laden constructs were cultured under a static state for 14 days before rhythmic strain was applied. Similarly, the TAA microphysiological model was constructed using the TAA HAoSMCs. After 14 days of maturation, the models were subject to the tensile strain for the following 7 days. A frequency of 1 Hz was chosen for all models. Microphysiological models that were incubated under static conditions for another 7 days (in total, 21 days) were control devices. Under all conditions, the culture medium (DMEM supplemented with 10% fetal bovine serum) was changed every other day. Following static and dynamic cultures, hydrogel samples were collected for staining, assessment of mitochondrial function, and quantitative real-time polymerase chain reaction (qRT-PCR).

Drug testing

Three medications that have been proven to delay or accelerate progression of aortic aneurysm in cellular and animal studies (metformin, losartan, and ciprofloxacin) were tested on the TAA microphysiological models with HAoSMCs derived from 8 TAA patients. Based on the previous pharmacokinetics studies on human subjects, metformin hydrochloride (PHR1084, Sigma-Aldrich), losartan potassium (IL0210, Solarbio), and ciprofloxacin hydrochloride (PHR1044, Sigma-Aldrich) were diluted with serum-free DMEM to their respective therapeutic concentrations reported in previous pharmacokinetic studies (metformin, 20 μM; losartan, 10 μM; and ciprofloxacin, 10 μM) and applied to the TAA models.[49-55] To simulate a hypothesized scenario where an overdose of ciprofloxacin was used to control infection in patients with renal dysfunction, a higher concentration of 100 μM was administered to the models. Medium with or without drugs was administered for 7 days of rhythmic strains (from Day 15 to Day 21) and changed daily for all models.

Cell viability assessment

The viability of cells encapsulated within the hydrogel was assessed using the LIVE/DEAD Viability/Cytotoxicity Kit (L3224, Invitrogen) according to the manufacturer's protocol. The devices were disassembled, and the hydrogels that stayed in between the inlets and outlets were removed. The remnant hydrogel was carefully peeled off the PDMS bottom layer. Afterwards, each sample was stained with a 200-μL solution of the two premixed dyes and incubated at 37°C for 45 minutes. Representative images of five different regions of each hydrogel were acquired using a fluorescence microscope (DMi8, Leica), and analyzed using the ImageJ software (ver. 1.52n, National Institutes of Health). Viability was calculated as live cell number / (live + dead) cell number × 100%.

Cytoskeleton staining and immunofluorescence

Cytoskeleton staining and immunofluorescence were performed on the models on Day 21. The hydrogel samples were fixed in 4% paraformaldehyde overnight at 4°C, permeabilized with 0.1% Triton-X (X100, Sigma-Aldrich) solution at room temperature for 1 hour and blocked using 5% bovine serum albumin. F-actin was stained with rhodamine phalloidin (R415, Invitrogen) for 90 minutes at room temperature on a shaker. The primary antibodies (TAGLN: ab14106, Abcam, RRID: AB_443021; BCL2: 60178-1-Ig, Proteintech, RRID: AB_10734459; ELN: AF6783, Beyotime, Shanghai, China; Collagen Type I: 67288-1-Ig, Proteintech, RRID: AB_2882554; AMPKα1/AMPKα2: AF6195, Beyotime; Phospho-AMPKα1/AMPKα2: AF5908, Beyotime) and secondary antibodies (4412S: Cell Signaling Technology, RRID: AB_1904025; 8890S: Cell Signaling Technology, RRID: AB_2714182; A21206: Invitrogen, RRID: AB_2535792) were incubated with the samples at 37°C

for 2 hours and 1 hour, respectively. After 5 times of washing with PBS, the nuclei were stained with 4′,6-diamidino-2-phenylindole (DAPI, D1306, Invitrogen) for 30 minutes at room temperature. Representative images of 3 different regions of each sample were acquired using a fluorescence microscope (DMi8, Leica) or a confocal microscope (TCS SP8 SR, Leica), and analyzed using the ImageJ software (ver. 1.52n, National Institutes of Health).

Immunohistochemical staining

The aortic issues and hydrogels were fixed using 4% paraformaldehyde at 4°C overnight, embedded with paraffin and cut into 4-μm sections. Before staining, all sections were subjected to antigen retrieval and blockings of endogenous peroxidase and non-specific binding sites. All slides were incubated with the primary antibodies (ACTA2: 19245, Cell Signaling Technology, RRID: AB_2734735; and MMP2: 40994, Cell Signaling Technology, RRID: AB_2799191) overnight at 4°C, and the secondary antibody (7074, Cell Signaling Technology, RRID: AB_2099233) at room temperature for 1 hour. 3,3-diaminobenzidine (K5007, Dako) was added to visualize the antigens *in situ*. The hematoxylin and eosin staining, Masson's trichrome staining, and Verhoeff–Van Gieson staining were performed according to the established protocols.[56]

Scanning electron microscopic imaging

Scanning electron microscopy (Phenom ProX, Thermo Fisher Scientific) was performed for assessment of the microstructure of the cell-laden hydrogels. After dissembling the PDMS chips, the hydrogels were washed with PBS, frozen at -80°C for 2 days, and lyophilized at -45°C for 5 days. The samples were coated with a thin platinum layer using a sputter coater for 30 seconds and loaded for imaging.

Proliferation and apoptosis assays

Cell proliferation and apoptosis were assessed using the Cell Counting Kit-8 (CCK8, C0038, Beyotime) and terminal deoxynucleotidyl transferase dUTP nick-end labeling (TUNEL, C10617, Invitrogen) assays, respectively. The cell-laden GelMA hydrogels cultured under static and strain conditions were incubated with CCK8 reagent at 37°C for 2 hours and loaded on a microplate reader (Allsheng, Shanghai). TUNEL assay was performed according to the manufacturer's protocols, and the samples were imaged using a confocal microscope (TCS SP8 SR, Leica).

qRT-PCR assays

The GelMA hydrogels were removed from the models, snap-frozen, and minced in liquid nitrogen. Total RNA of cells encapsulated within the hydrogels were extracted using TRIzol agent (T9424, Sigma-Aldrich). To characterize the gene expression profile of the native aortic medial layer, the nondiseased and TAA tissues were dissected, and the RNA of medial layer tissue was extracted using a similar approach. Synthesis of complementary DNA and qRT-PCR were performed according to standard protocols (RR037B and RR420B, Takara). The primers used in this study were listed in Supplemental Tables 2 and 3.

Mitochondrial staining

Mitochondrial membrane potential was assessed using Image-iT^{TM} TMRM Reagent (I34361, Invitrogen), a cell-permeable dye that accumulates in mitochondria with high membrane potential. MitoSOX^{TM} Red mitochondrial superoxide indicator (M36008, Invitrogen; Ex/Em: 510/580 nm) was used to detect superoxide in the mitochondria of live cells and on frozen sections of aortic tissues. All staining was performed according to the manufacturer's protocols. Counterstaining was performed using DAPI (D1306, Invitrogen) or Mitotracker Red (M22425, Invitrogen).

Mitochondrial respiration assessment

The hydrogels encapsulating control and diseased HAoSMCs were planted onto the XF96 plates using a microfluidic puncher (diameter: 4 mm). Cells cultured in 2D flasks were planted according to the manufacturer's protocols. Oxygen consumption rates (OCRs) and extracellular acidification rates (ECARs) were measured using the mitochondrial stress test kit (103015-100, Agilent) with the following drug concentrations: 1.5-μM oligomycin, 2-μM FCCP and 0.5-μM rotenone + antimycin A, on the XF96 Extracellular Flux Analyzer (Seahorse Bioscience, Agilent) as previously described[57]. OCRs and ECARs were normalized by the amount of the total DNA extracted using TRIzol agent (T9424, Sigma-Aldrich). Cytosolic nicotinamide adenine dinucleotide (NAD^+)/nicotinamide adenine dinucleotide hydride (NADH) ratio was measured using NAD^+/NADH quantification kit (S0175, Beyotime).

Mouse experiments

All protocols of animal experiment were approved by the Animal Care and Ethics Committee of Fudan University (approval number No. 202112010S), and all procedures conformed to the Guide for the Care and Use of Laboratory Animals guidelines. Three-week-old wild type C57BL/6J male mice were grouped into 3 groups (Group A, untreated control; Group B, β-aminopropionitrile (BAPN) + saline; and Group C, BAPN + metformin), which were designated by W.M. The study groups were not blinded to researchers, and there was no criterion for including or excluding

animals. The Group B mice were administered BAPN (6 g/l) dissolved in drinking water, and the Group C mice received BAPN (6 g/L) and metformin (300 mg/l) in drinking water. On Day 28, the surviving animals were euthanized by cervical dislocation. The thoracic aortic tissues were collected from prematurely dead animals and from those surviving 28 days of drug treatment, with consistent harvesting methods. The event of hemothorax caused by aortic dissection/rupture was recorded, and the maximal diameters of ascending aorta, aortic arch and descending aorta were measured. The tissues were fixed, paraffin-embedded, sectioned, and underwent hematoxylin and eosin staining, Alcain blue staining, and Verhoeff–Van Gieson staining. NAD^+ quantification and qRT-PCR were performed as aforementioned. All tissues in the control and experimental groups were harvested and included in the analysis by W.M. and J.Z.

Clinical data collection and analyses

In this study, collection of clinical and imaging data of hospitalized patients were conducted in a retrospective manner, for which the requirement of informed consent was waived (Zhongshan Hospital Fudan University Ethics Committee Approval Letter No. B2020-158R). Between January 2015 and August 2020, in the Department of Cardiac Surgery of our institution, a total of 1566 patients were identified with a bicuspid aortic valve, a common congenital heart malformation associated with TAA. Among them, 137 (8.7%) patients were diagnosed as being diabetic. Fifty-six (40.9%) patients had a history of receiving isolated or combined metformin therapy for blood glucose control and the others did not. We screened 137 non-diabetic patients to match the diabetic patients in an age and sex-dependent manner. Ascending aortic diameter of each patient was measured using chest computed tomography by two independent investigators blinded to patient's medical history, which was further indexed by patient's body surface area to control bias. Baseline characteristics, comorbidities, valvular function, concomitant medications, and aortic size were documented and compared between patients with and without metformin. Univariate linear regression was performed to assess risk factors for raw and indexed ascending aortic diameters, respectively, in diabetic and non-diabetic patients (n=274). Variables with P value < 0.15 were further included in multivariate models for confounder-adjusted analysis.

Statistical analysis

Continuous variables were presented as means ± standard deviations or median (interquartile range), according to the normality test. Parameters were compared using the two-tailed Student's t-test (normal distributions) or the Mann-Whitney U-test (non-normal distributions). Multiple intergroup comparisons were performed using the one-way analysis of variance (ANOVA) with Dunnett's correction for multiple comparisons. Categorical variables were expressed as numbers (percentages) and compared using chi-square test. Survival analysis was performed using the log-rank test. Analyses were performed using GraphPad Prism v8.0 (GraphPad Software Inc.) and SAS v8.0 (SAS Institute Inc.) software. Statistical significance was indicated by $^{ns}P > 0.05$, $^{*}P < 0.05$, $^{**}P < 0.01$, and $^{***}P < 0.001$, respectively.

Reagent validation

All chemical reagents and antibodies used in this study were common and commercially available. The detailed information of the antibodies was listed in the Reagent Validation File. These antibodies have been validated in the immunofluorescence and immunohistochemical assays in multiple previous studies, and no specific validation test was performed in the current study. Nevertheless, positive correlations of gene expressions were detected by the antibodies and by qRT-PCR assays.

Role of funding source

The funding sources did not involve in any aspect pertinent to the study.

Results

Microphysiological system for 3D dynamic cell culture

The microstructure of the aortic medial layer is composed of undulated elastin layers (lamellae) and sandwiched, aligned HAoSMCs, which rhythmically relaxes and tensions in cardiac cycles (Figure 1a, 1b). The mean strain of the aortic wall ranges between 6.7% and 13.8%,[58,59] which can be further influenced by age, aortic diameter, and the presence of aortic disease.[60-62] Based on previous studies, a mean circumferential strain of 10% was considered physiological and replicated on this microphysiological model (Figure 1b).[58,59,62-64] We first aimed to emulate the biological and biomechanical microenvironment of HAoSMCs in the medial layer of the thoracic aorta. We designed a microelectromechanical system to apply confined rhythmic tensile strain to a 3D, HAoSMC-laden hydrogel construct, which mimicked aortic expansion and relaxation during cardiac systole and diastole. The fabricated device was composed of two plasma-bonded PDMS slabs enveloping a cell culture chamber (Figure 1c). The upper part of the chamber was a reservoir for culture medium. The inner surface of the lower part was polydopamine-treated to increase hydrophilicity and hydrogel adhesion and used as the strain compartment for stretching the cell-laden artificial tissue (Figure 1d, Supplemental Figure 1). Multiple cylindrical pillars were protruding from the bottom of the lower slab. A stepper motor was used to impose rhythmic bilateral elongation to the PDMS chip, generating displacement

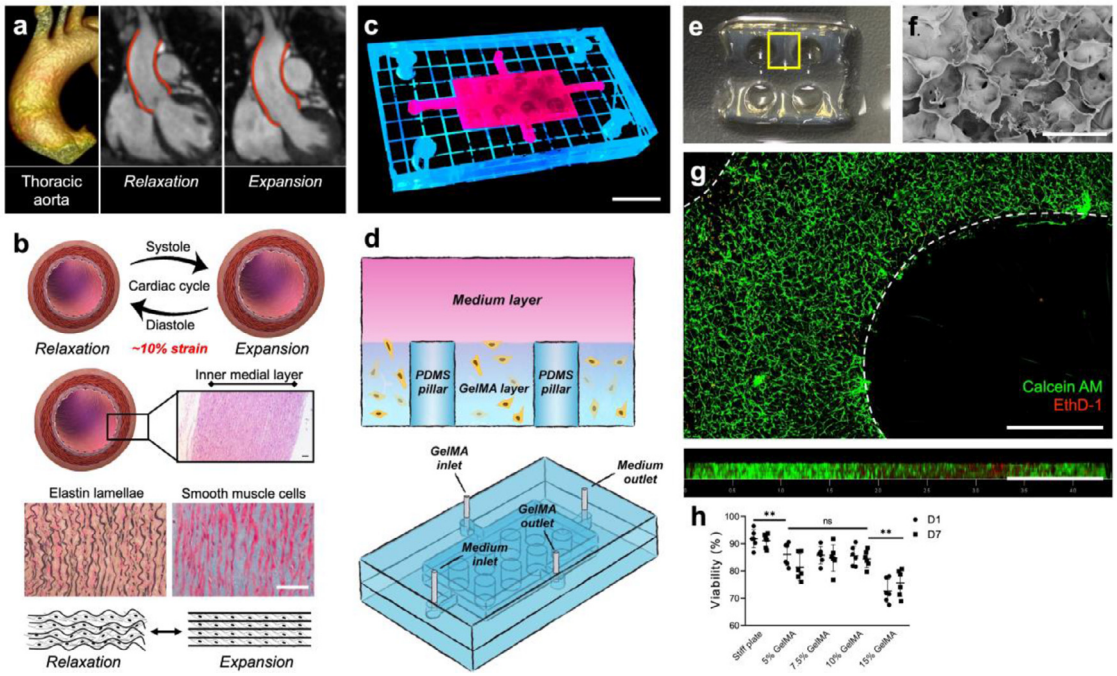

Figure 1. Construction of the aortic microphysiological model. (a) Within a cardiac cycle, the human aorta expands with ejected blood flow at systole and relaxes at diastole, with a mean physiological strain of approximately 10% in the ascending thoracic aorta. **(b)** This microphysiological model was designed to emulate such a cyclic strain imposed on the aortic tunica media (hematoxylin and eosin), which was composed of elastin lamellae (black, Verhoeff-Van Gieson staining) and sandwiched smooth muscle cells (red, Masson' trichrome staining). Scale bar: 50μm. **(c)** Image of an assembled microphysiological model. Scale bar: 1 cm. **(d)** The microphysiological model was composed of two PDMS slabs polymerized in molds. HAoSMC-encapsulated GelMA solution was injected into the model and crosslinked. The device was incubated under static conditions for 14 days (maturation) and underwent rhythmic strain for another 7 days. On day 21, the hydrogels within the models were harvested and subjected to analyses. **(e, f)** Macroscopic and scanning electron microscopic images of the GelMA-based hydrogel. Scale bar: 80µm. **(g)** Live/dead staining of HAoSMCs within the hydrogel imaged by a confocal microscope. Calcein AM staining (green) indicates live cells and EthD-1 staining (red) indicates dead cells. Scale bar: 1mm. **(h)** Cell viabilities in hydrogels with different GelMA concentrations (n=6 including 3 biological replicates; ANOVA). Values are presented in means ± standard deviations. ns, $P > 0.05$; **, $P < 0.01$.

between pillars that deformed the attached hydrogel (Supplemental Figure 2; Supplemental Video 1).

The control HAoSMCs were harvested and expanded from aortic tissues of 3 patients who underwent cardiac surgery with a normal aortic valve and thoracic aorta (patient details listed in Supplemental Table 1). The cell-laden GelMA solution was injected into the device and crosslinked. The porous microstructure of GelMA hydrogel, with adequate structural strength to maintain an intact morphology after rhythmic strain and extraction from the PDMS model, allowed cellular attachment, expansion and exchange of nutrient and waste (Figure 1e, 1f). Live/dead staining showed favorable viabilities of HAoSMCs (Figure 1g, 1h).

Strain distribution in the cell-laden hydrogel

The strain distribution within the hydrogel was simulated using finite element analysis. A total of 6 configurations of pillar arrays was calculated, which showed that the hydrogel driven by the 2 × 4 cylindrical pillars received an average of ~10% strain along the stretching direction, with trivial compression on the orthogonal axes (Figure 2a; Supplemental Table 4). Further, we added carbon fibers into the GelMA mixture before crosslinking to assess the strain distributions within the hydrogel and to compare with the results of computational simulation. A similar methodology has been reported in previous studies.[16] The carbon fibers used in this study were 5 μm in diameter and 48 μm in length (Supplemental Figure 3). The results showed that region A had the highest X-axis strain and Y-axis compression, and region C had the lowest X- and Y-axis strains, which were consistent with the computational simulations (Supplemental Figure 3). These data demonstrated that a physiological strain was well-conducted within the cell-laden hydrogel.

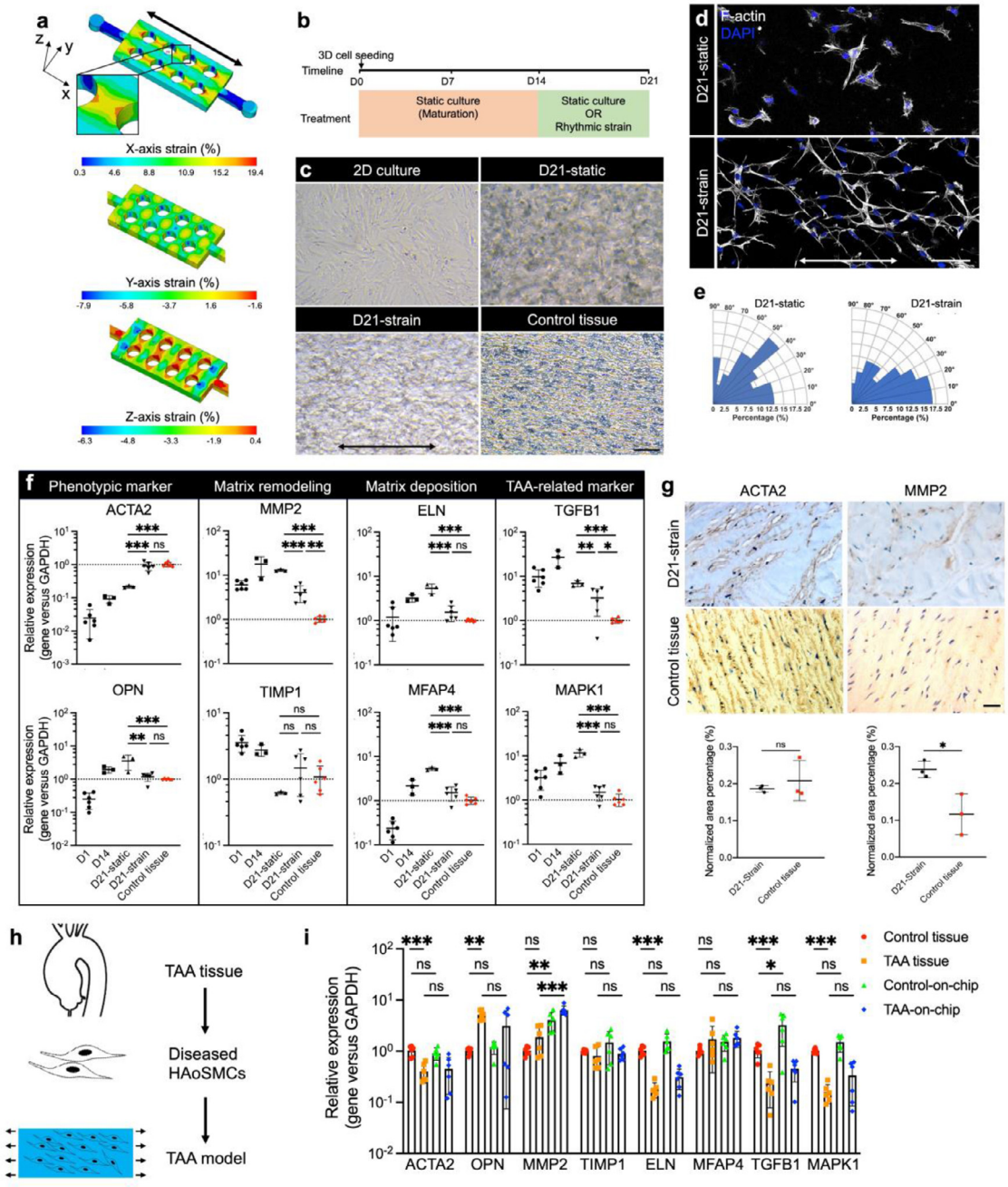

Figure 2. Biomechanical and biological validation of the microphysiological model. (a) Finite element analyses of the strain distribution on the long axis demonstrated that the model with 2 × 4 cylindrical pillars had low strain deviation on the X-axis and trivial strains on the Y- and Z-axes. The black arrow indicated strain direction. **(b)** The HAoSMC-laden, GelMA-based microphysiological models underwent 14 days of static incubation (maturation), followed by 7 days of static culture or rhythmic strains. **(c)** Morphologies of HAoSMCs cultured under different conditions and in the native tissue. Cells under 2D culture were excessively expanded, and cells under dynamic, 3D culture had similar size and orientation to those in the aortic tissue. Scale bar: 50 μm. **(d)** Confocal images of F-actin (white) and nuclei (blue) staining on day 21 in static and strain models. The black arrows indicated the strain direction. Scale bar: 50 μm. **(e)** Radar diagrams showing distributions of cellular orientations relative to the strain direction. HAoSMCs in the strain models were prone to align parallel to the strain direction. **(f)** Compared with the control aortic tissue, HAoSMCs that underwent 7 days of rhythmic strain exhibited similar expression of the ACTA2, OPN, TIMP1, ELN, MFAP4, and MAPK1 (n=3−6 with 3 biological replicates; ANOVA). The expression levels of MMP2 and TGFB1 were significantly increased in the aorta-on-model model (n=6 with 3 biological replicates; ANOVA). **(g)** Immunohistological staining showing that the protein level of ACTA2 was comparable

Morphological changes of cells under 3D dynamic culture

After cell seeding onto the models, the models were cultured for 14 days under a static state, followed by 7 days of rhythmic tensile strain (Figure 2b). During the 21 days of culture, the control and TAA-derived HAoSMCs did not proliferate significantly (Supplemental Figure 4), which were consistent with previous studies showing that under 3D physiological cyclic strain, the primary vascular smooth muscle cells exhibited a quiescent, nonproliferating state.[65-67] Compared with cells cultured under static 2D condition, the cells under 3D culture and in the human aortic tissue were smaller in sizes. With tensile strain, the HAoSMCs aligned along the strain direction, which were similar to those in the tissue (Figure 2c). With prolonged culture time, the cells on the model became better spread and assembled more F-actin fibers (Figure 2d). F-actin staining showed irregular orientation of cells cultured under static 3D condition, while on the dynamic 3D model, HAoSMCs exhibited spindle-like morphologies with more established intercellular connections and anisotropic alignment with the strain direction (Figure 2e). We observed cell elongation on Day 1, and orientation parallel to the strain direction on Day 3 and Day 7 (Supplemental Figure 5). Elastin and collagen type I, two major components of the aortic matrix, were synthesized and deposited by HAoSMCs cultured under static and strain conditions (Supplemental Figure 6). Elastin was better-retained within the matrix in the strain group, despite that expression of ELN was higher in cells under 21 days of static culture (Figure 2f). This phenomenon suggested that insoluble elastin was better-preserved in the extracellular matrix surrounding cells under rhythmic strain, which was also reported in previous studies.[68,69] All these observations were physiologically featured in the human aortic tissue.

Expressions of TAA-related genes on the microphysiological model

To assess the expressions of TAA-related genes in the model, we performed qRT-PCR analysis using differently cultured cells and the control aortic medial layer tissue (Figure 2f). We selected 8 genes as phenotypic HAoSMC markers, including alpha-smooth muscle actin (ACTA2), osteopontin (OPN), matrix metalloproteinase 2 (MMP2), tissue inhibitor of matrix metalloproteinase 1 (TIMP1), elastin (ELN), microfibril-associated glycoprotein 4 (MFAP4), transforming growth factor beta 1 (TGFB1) and mitogen-activated protein kinase 1 (MAPK1). Of these genes, ACTA2, MMP2, TIMP1 and ELN are well-established genes associated with aortic aneurysm, and the other 4 genes (OPN, MFAP4, TGFB1 and MAPK1) are reported markers in aneurysmal smooth muscle cells.[3,70-74] Specifically, MFAP4 is an extracellular matrix protein that is involved in cell adhesion or intercellular interactions. Previous studies have shown that upregulation of MFAP4 is a compensatory response to the abnormal elastin formation in Marfan syndrome patients, and lower MFAP4 protein expression in abdominal aortic aneurysm reflects the increased expression of proteases or the loss of contractile vascular smooth muscle cells.[72,75] On Day 21, HAoSMCs that underwent rhythmic strain (D21-strain) exhibited enhanced expression of contractile phenotypic marker ACTA2, which was comparable to that in normal aortic tissues. OPN, ELN, MFAP4, TIMP1, and MAPK1 were also comparably expressed on the dynamic microphysiological models and in normal aortic tissues. The expressions of MMP2 and TGFB1 were higher on the model, which might be attributed to the ongoing process of extracellular matrix remodeling. Expressions of these genes were significantly different from the control tissue in HAoSMCs on the 3D static models (D21-static), and at least 21 days of maturation were required to achieve the present emulation (Supplemental Figure 7). The expressions of ACTA2, OPN, MMP2, and TIMP1 were comparable at different sites of the hydrogel (Supplemental Figure 8). Immunohistological staining demonstrated that the nondiseased HAoSMCs on the microphysiological model exhibited comparable expression of ACTA2 and increased expression of MMP2 compared with cells in tissue (Figure 2g).

Subsequently, we expanded diseased HAoSMCs from TAA tissues and planted them into the construct to establish TAA microphysiological models (Figure 2h). Similar to cases in the normal (nondiseased) 3D models, the diseased HAoSMCs on the models showed comparable expressions of phenotypic markers, TIMP1, matrix remodeling markers, and TAA-related markers with those in the TAA tissues, and only MMP2 was significantly upregulated (Figure 2i). These results suggested the model's capability of recapitulating the *in vivo* pathophysiology of HAoSMCs.

Mitochondrial dysfunction and phenotypic switching were highlighted on the microphysiological models

To evaluate the impact of the 3D dynamic model on cell phenotypes, the expressions of TAA-related genes were assessed in control and diseased HAoSMCs cultured under 2D and 3D conditions (Figure 3a). We observed

between the cells in the hydrogel and the normal tissue, while the level of MMP2 was higher on the microphysiological model (n=3 with 3 biological replicates; ANOVA). Scale bar: 50 μm. **(h)** Schematic diagram of cells harvested from TAA tissues and planted on microphysiological models. **(i)** Five out of the 8 TAA-related genes were differently expressed between the control and TAA tissues. Genes other than MMP2 were comparably expressed between the TAA tissues and the TAA models (n=3−6 with 3 biological replicates; ANOVA). Values are presented in means ± standard deviations for all panels. ns, $P > 0.05$; *, $P < 0.05$; **, $P < 0.01$; ***, $P < 0.001$.

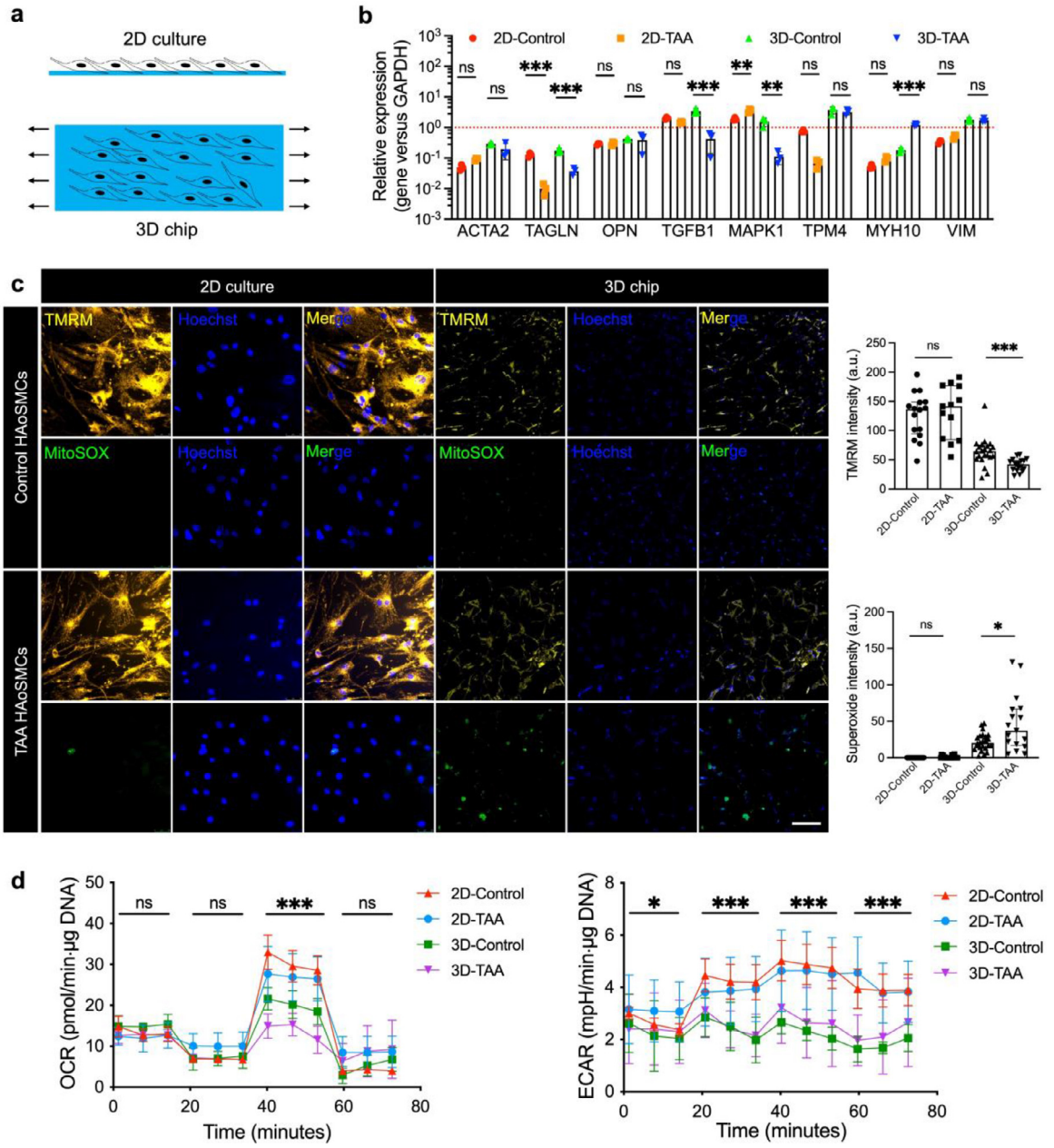

Figure 3. Phenotypic switching and mitochondrial dysregulation were observed in cells cultured on microphysiological models, but not in those in flasks. (a) Schematic diagram of cells cultured on microphysiological models and in flasks (2D static culture). **(b)** qRT-PCR assays showing that under 2D culture, ACTA2, OPN, TPM4, MYH10 and VIM were comparably expressed in control aorta- and TAA-derived cells. On 3D dynamic models, the diseased cells expressed lower TAGLN, TGFB1 and MAPK1, and higher MYH10 (n=3 with 3 biological replicates; ANOVA). **(c)** Mitochondrial membrane potential assessed by TMRM staining, in together with superoxide level, were comparable between nondiseased and diseased HAoSMCs under 2D culture, while the differences were highlighted when cells were cultured on the dynamic 3D model: the TAA HAoSMCs exhibited significantly lower mitochondrial membrane potential and higher superoxide level than control (n=13−24; including 2 biological replicates; t-test). Scale bar: 50 μm. **(d)** Mitochondrial respiration stress assays showing that mitochondrial function was more intensely challenged in cells on the models, where diseased HAoSMCs had impaired function of oxidative phosphorylation (n=3 including 3 biological replicates; ANOVA). Values are presented in means ± standard deviations for all panels. ns, $P > 0.05$; *, $P < 0.05$; **, $P < 0.01$; ***, $P < 0.001$.

that in the culture flask, the control and TAA-derived HAoSMCs expressed comparable levels of ACTA2, OPN, TGFB1, tropomyosin 4 (TPM4), myosin heavy chain 10 (MYH10) and vimentin (VIM), while on the microphysiological device, the expressions of transgelin (TAGLN), TGFB1 and MAPK1 were significantly lower in the diseased cells (Figure 3b).

Recent research has shown that mitochondrial dysfunction may be an important hallmark in the development of TAA.[33-35,76] Abnormal expression of mitochondrial genes, a lower number of mitochondria and overaccumulation of superoxide were also observed in TAA tissues (Supplemental Figure 9). When cultured in 2D flasks, the control and diseased cells showed similar mitochondrial membrane potentials and comparably low levels of intracellular superoxide (Figure 3c). However, on the 3D dynamic model, the diseased cells exhibited a lower mitochondrial membrane potential and a higher level of superoxide compared with control. Analysis of cellular respiration showed that cells in flasks exhibited higher levels of OCR and ECAR than those on the models (Figure 3d). Whilst peak OCR after FCCP treatment was comparable between control and diseased HAoSMCs in the flasks, such parameter was significantly decreased in the diseased cells under 3D dynamic culture. These data indicated that cells were more mitochondrially challenged on the 3D microphysiological models, where the diseased HAoSMCs exhibited more remarkable impairment in mitochondrial function and phenotypic switching than on 2D static models.

To further demonstrate the recapitulative ability of the 3D dynamic model, we compared the expressions of TAA-related genes, mitochondrial membrane potential and superoxide in cells cultured under 2D and 3D dynamic conditions (Supplemental Figure 10). For 2D strain culture, the resuspended HAoSMCs were injected on a tensile membrane and allowed to grow statically for 14 days before the 7-day rhythmic stretching was applied, using the 2D dynamic device previously reported by our group.[77] In the 3D microphysiological model, the expression of ACTA2 in control and TAA-derived cells was significantly elevated compared with 2D strain culture. The expressions of CNN1 and ELN were upregulated in the diseased cells under 3D dynamic culture. Both under 2D and 3D strain culture, mitochondrial membrane potential was significantly higher in the control cells than in TAA-derived cells. In the 2D dynamic model, superoxide accumulation was comparable between control and diseased cells, while in the 3D model the difference was significant. These findings suggested that both 2D and 3D dynamic models were physiologically relevant, while the 3D microphysiological models better recapitulated the expressions of contractile markers and highlighted superoxide accumulation in TAA models.

Drug testing on individualized TAA models

After studying the pathophysiological relevance of the model, we aimed to test the effects of 3 drugs (Figure 4a) on personalized TAA models of 8 patients (patient details listed in **Supplemental Table 1**). Based on the existing literature.[70,72,78-81] and the comparison between TAA and control aortic tissues (Figure 2i), in the patient-derived TAA microphysiological models, upregulation of ACTA2, TIMP1, ELN, MFAP4, TGFB1 and MAPK1 was considered potentially beneficial for controlling TAA, and upregulation of OPN and MMP2 was presumably harmful. Metformin and losartan are two drugs associated with delayed progression of abdominal aortic aneurysm and Marfan syndrome-related aortic aneurysm, respectively [9,41]. Ciprofloxacin is a broad-spectrum antibiotic recently shown to increase the risks of aortic aneurysm and dissection [82] (Figure 4a). Drug testing was performed on the models treated using metformin (20 μM), losartan (10 μM), and ciprofloxacin (10 μM and 100 μM) for 7 consecutive days, according to their circulatory concentrations reported in literature [49-55]. After drug treatment, metformin exhibited remarkable upregulation of contractile marker ACTA2, TIMP1, and TGFB1, showing a general tuning effect (Figure 4**b**). Expression of another contractile marker of HAoSMC, TAGLN, was also increased after metformin treatment (Supplemental Figure 11). Losartan impacted little on the abnormal expressions of the TAA-related genes (Figure 4b). While a low dose of ciprofloxacin elevated MFAP4 expression, a higher ciprofloxacin concentration was associated with impairment in contractile phenotype, synthesis of ELN and MFAP4, and upregulation of TGFB1 (Figure 4b). These results indicated a potentially beneficial effect of metformin on the TAA HAoSMCs. Losartan failed to yield a significant ameliorative effect, and the detrimental impact of high-dose ciprofloxacin on HAoSMCs was shown.

Recovery of mitochondrial dysfunction after metformin treatment

Apart from its antidiabetic effect, supra-pharmacological dose of metformin has been reported to inhibit proliferation of cancer cells by blocking mitochondrial respiratory complex I.[83,84] Given the enormous difference in metabolic behavior between cancer cells and HAoSMCs, and the uneven distribution of metformin in human tissues, we further evaluated the effect of metformin on mitochondrial function of HAoSMCs. It was observed that a therapeutic concentration of metformin (20 μM) led to increased mitochondrial membrane potential and decreased superoxide accumulation in both control and TAA-derived cells (Figure 5a). We compared the immediate OCR changes in control and TAA HAoSMCs in response to vehicle and 20 μM metformin, which showed an increase in maximal OCR after metformin treatment (Figure 5b). The baseline and maximal ECARs were also significantly increased (Figure 5b). The NAD^+/NADH ratio was elevated by

a

Drug	Classification	Effect on aortic health	Effect on nonfamilial TAA	Possible target
Metformin	Antidiabetic	Abdominal aortic aneurysm↓	Unknown	AMPK pathway/mitochondrial activity
Losartan	Antihypertensive	Marfan syndrome aortic aneurysm↓/→	Unknown	TGF-β pathway
Ciprofloxacin	Antibiotic	Aortic aneurysm/dissection↑	Probably aggravating	Mitochondrial DNA damage

b

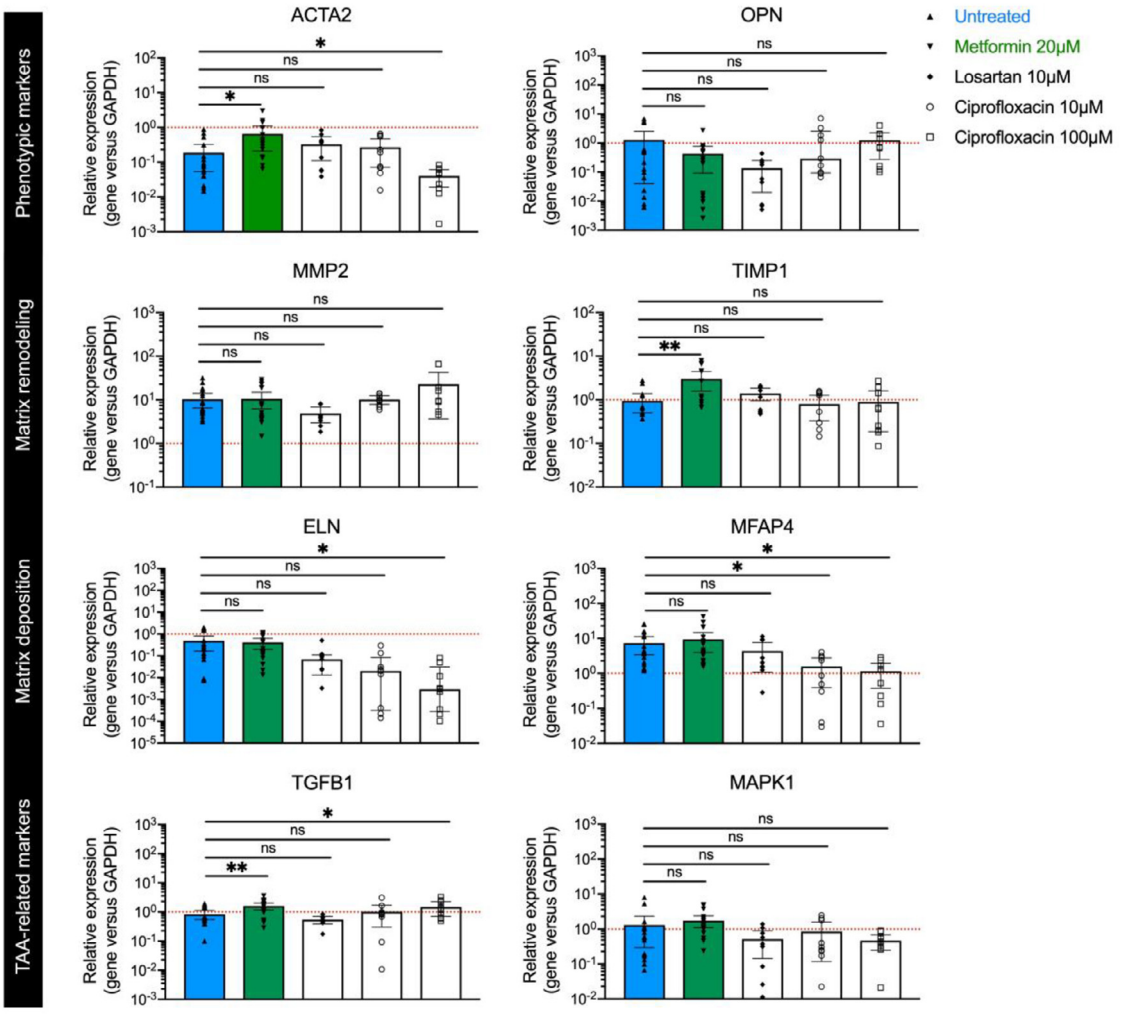

Figure 4. Drug testing on the microphysiological models. (a) Brief summary of the 3 drugs to be tested on the models. Preliminary clinical studies have shown the possibilities of metformin and losartan to control aortic aneurysm, and ciprofloxacin may accelerate aneurysm progression. **(b)** Drug testing was performed using HAoSMCs harvested from samples of 8 TAA patients. Doses of drugs were administered according to their therapeutic concentrations in the human peripheral blood. Metformin, at a concentration of 20 μM, was associated with elevated levels of ACTA2, TIMP1 and TGFB1. Losartan (10 μM) did not significantly influence the expressions of the TAA-related genes. While a lower dose (10 μM) of ciprofloxacin only reduced MFAP4 expression, a higher dose (100 μM) significantly changed the expressions of ACTA2, ELN, MFAP4, and TGFB1 (n=9−17 with 8 biological replicates; ANOVA). Red dot lines indicate the expression levels of the control aortic tissues. Values are presented in means ± standard deviations for all panels. ns, $P > 0.05$; *, $P < 0.05$; **, $P < 0.01$.

metformin, suggesting recovery of the NAD^+ pool that was reported to be important to HAoSMC homeostasis[85,86] (Figure 5c). Compared with the untreated models, the expressions of AMP-activated protein kinase alpha 1 gene (PRKAA1), mitochondrial respiratory complex V component ATP synthase F1 subunit alpha (ATP5F1A), BCL2 apoptosis regulator (BCL2), and translocase of outer mitochondrial membrane 20 (TOMM20) were significantly upregulated after metformin treatment (Figure 5d). The expression of PRKAA1-encoded protein, AMPKα1, as well as its phosphorylated form p-AMPKα1, was upregulated after

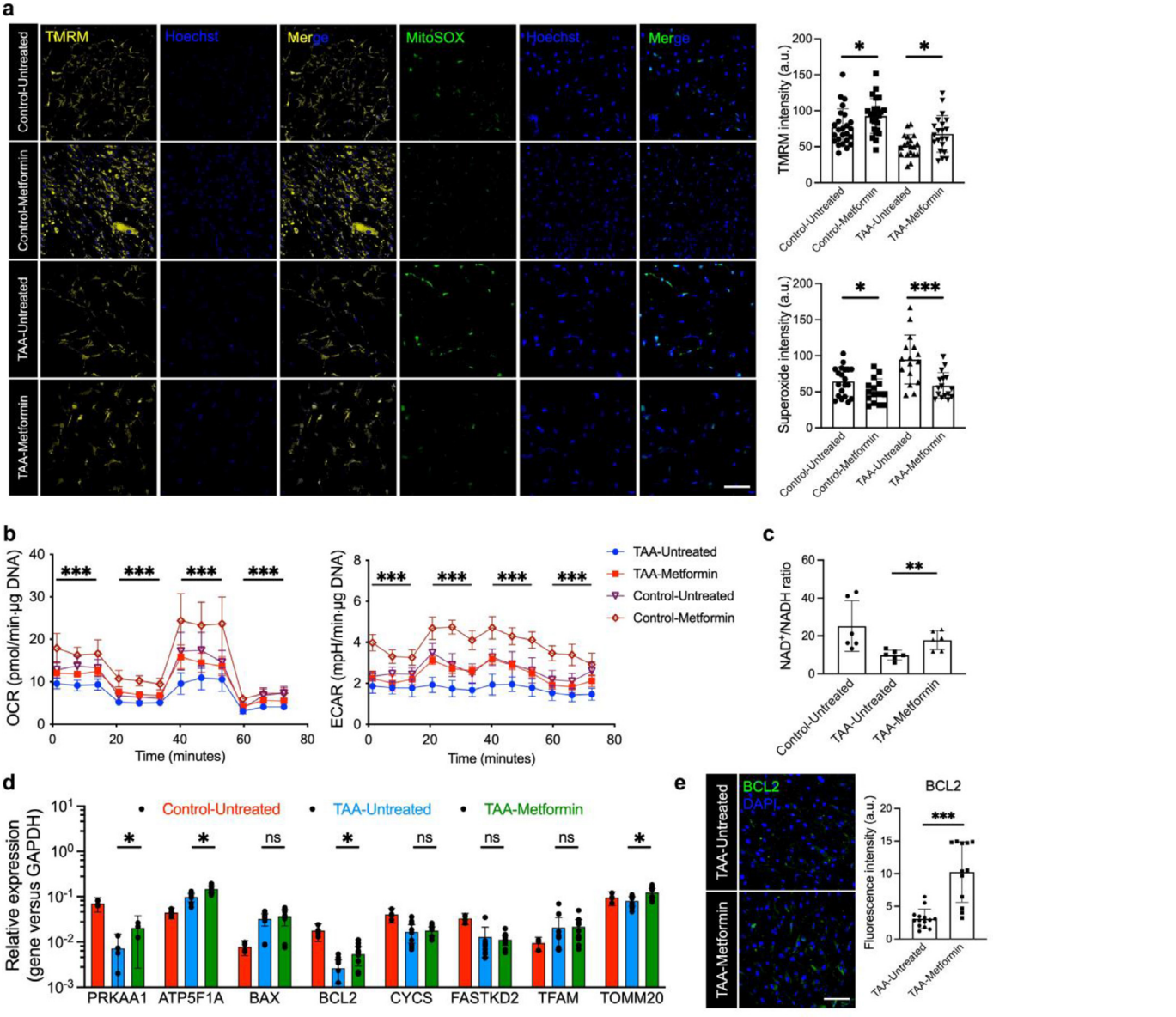

Figure 5. Metformin's effect on mitochondrial health of TAA HAoSMCs. (a) Metformin significantly increased mitochondrial membrane potential (TMRM intensity) in TAA HAoSMCs and in control cells. This drug significantly reduced the superoxide levels in both diseased and nondiseased cells (n=15−25 including 2 biological replicates; ANOVA). Scale bar: 50 μm. **(b)** Mitochondrial respiration stress test showing elevation in maximal OCR and baseline and maximal ECAR in both control and TAA cells after metformin treatment than those without (n=3−9 including 3 biological replicates; ANOVA). **(c)** The cytosolic NAD^+/NADH ratio was significantly elevated after metformin treatment (n=6 including 3 biological replicates; ANOVA). **(d)** qRT-PCR assays showing that metformin elevated the expressions of several mitochondrial genes on the models (n=5−8 including 3 biological replicates; ANOVA). **(e)** Immunofluorescence showing an increased BCL2 expression after metformin treatment (n=12−14 including 2 biological replicates; ANOVA). Scale bar: 50 μm. Values are presented in means ± standard deviations for all panels. ns, $P > 0.05$; *, $P < 0.05$; **, $P < 0.01$; ***, $P < 0.001$.

metformin treatment Supplemental Figure 12). The intracellular BCL2 protein level was also increased (Figure 5e). However, apoptosis in the untreated TAA-derived HAoSMCs was at a relatively low level that did not significantly differ from the control cells, or the TAA-derived cells treated with metformin **(Supplemental Figure 13)**.

Metformin's effect on murine TAA models

To validate the beneficial effect of metformin *in vivo*, we tested the drug response on established murine TAA models[30]. We treated 3-week-old wild type C57BL/6J mice with 1) saline (n=5), 2) BAPN (6 mg/ml) + saline (n=12), and 3) BAPN (6 mg/ml) + metformin (300 ug/ml) (n=12; Figure 6a). After 4 weeks of treatment, TAA

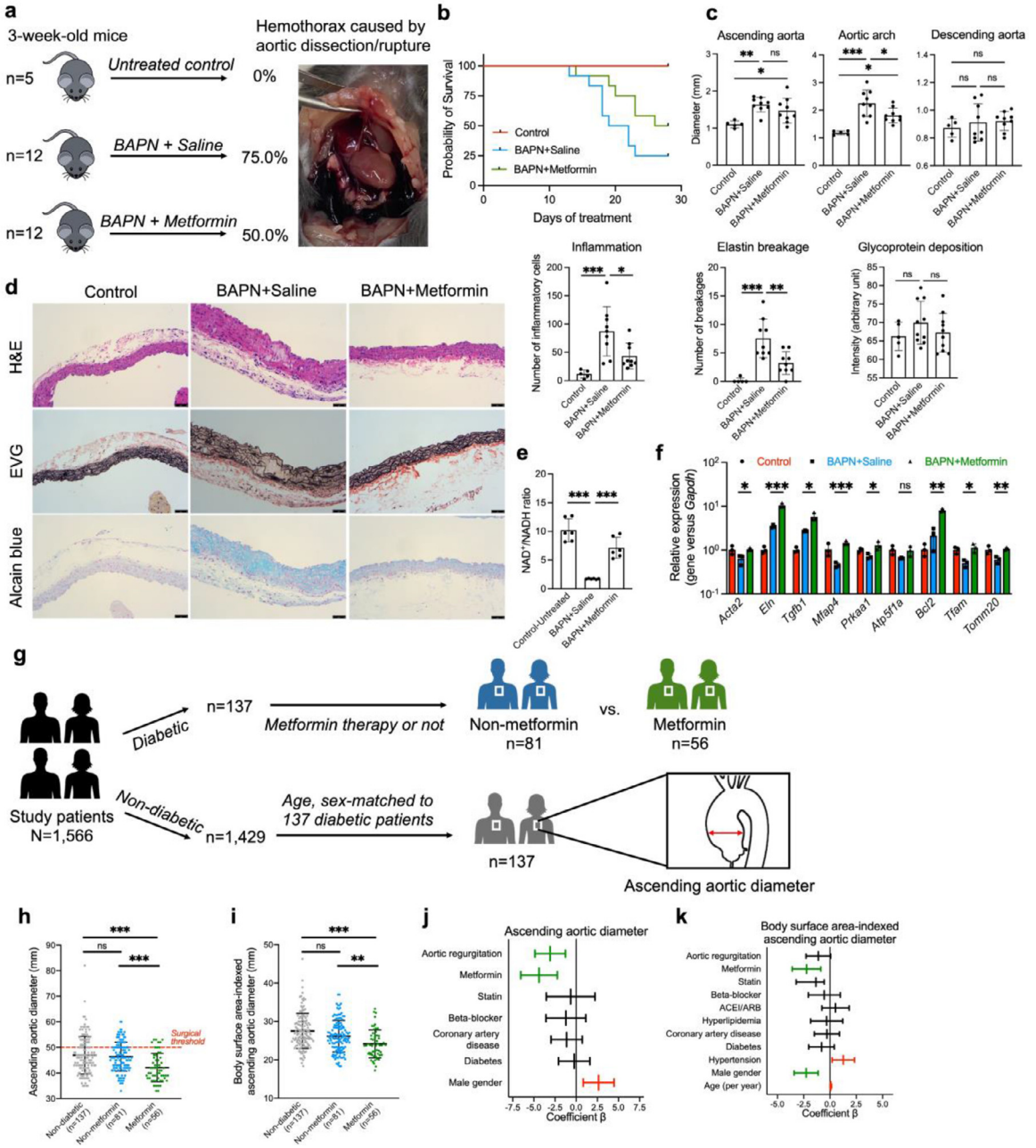

Figure 6. ***In vivo*** **validation of metformin's effect on TAA development. (a)** Young wild type C57BL/6J mice were treated with saline only, BAPN + saline and BAPN + metformin for 4 weeks. Hemothorax, indicative of aortic dissection or rupture, presented in more than half of the mice treated with BAPN + saline and only in 1 mouse treated with BAPN + metformin. **(b)** Survival analysis of the 3 groups (N=29; log-rank test, P=0.108). **(c)** Aortic dilation is evident across all sections in BAPN-treated mice, and metformin significantly delayed dilation of the aortic arch (n=5−12 including 5−12 biological replicates; ANOVA). **(d)** Hematoxylin and eosin (H&E), Verhoeff's Van Gieson, and Alcain blue staining of the mouse aortic tissues showed that metformin reduced the excessive inflammatory cell invasion and elastin breakage (n=5−9 including 4 biological replicates; ANOVA). Scale bar: 100 μm. **(e)** Metformin partially recovered the NAD^+ pool that was depleted by BAPN treatment (n=6 including 3 biological replicates; ANOVA). **(f)** qRT-PCR analysis suggested elevated expressions of *Acta2, Eln* and multiple mitochondrial genes after metformin treatment (n=3 including 3 biological replicates; ANOVA). **(g)** Flowchart illustrating the screening of patients. **(h, i)** Comparisons of the raw and body surface area-indexed ascending aortic diameters showed that the patients who received metformin for glucose control had smaller aortic sizes than the diabetic patients without metformin and the non-diabetic patients (N=274). **(j, k)** Univariate and multivariate linear regression models demonstrated that the use of metformin was an independent factor associated with lower raw and indexed

was identified in 10 (83.3%) mice treated with BAPN + saline, and in 7 (58.3%) mice treated with BAPN + metformin (chi-square test, P=0.371). Lethal aortic dissection or rupture was identified in 6 (50.0%) mice with metformin and in 9 (75.0%) mice without (Figure 6b, log-rank test, P=0.108). The maximal aortic diameters at different aortic levels were compared across groups (Figure 6c), which showed that metformin significantly attenuated dilation of the aortic arch, while such effect was not evident in the ascending aorta and descending aorta. The aortic samples were subject to hematoxylin and eosin, Verhoeff's Van Gieson, and Alcain blue staining (Figure 6d). Invasion of inflammatory cells and elastin breakage were more prominent in tissues with BAPN + saline treatment, while degree of glycosaminoglycan deposition was comparable across three groups. The NAD^+/NADH ratio, and expressions of *Acta2, Eln, Tgfb1, Mfap4, Prkaa1, Bcl2, Tfam* and *Tomm20*, were also elevated by metformin (Figure 6e, 6f).

Clinical correlation between metformin usage and TAA development

Finally, we conducted a cross-sectional study to evaluate whether a history of metformin therapy would lead to delayed aortic dilation in patients with bicuspid aortic valve, a common contributing factor for TAA. Since the current on-label use of metformin is limited to patients with type 2 diabetes, we screened 137 diabetic patients and 137 age and sex-matched non-diabetic counterparts from a total of 1566 consecutive adult candidates hospitalized at our department from 2015 to 2020 (Figure 6g), and retrospectively collected the raw and body surface area-indexed ascending aortic diameters and other clinical characteristics. Unadjusted analyses indicated that patients with (n=56) and without (n=81) metformin therapy had comparable baseline demographics, comorbidities, and histories of medications (Supplemental Table 5). Both raw and body surface area-indexed ascending aortic diameters were comparable between non-diabetic patients and diabetic patients without metformin therapy, but were significantly lower in patients with metformin therapy compared with the other two groups (ANOVA, both P<0.05; Figure 6h, 6i), in whom the rate of TAA (raw ascending aortic diameter exceeding 50 mm) was remarkably lower (metformin versus non-metformin, 16.1% versus 30.9%, chi-square test, P=0.049) [87]. Multivariate linear regression models for raw and indexed ascending aortic diameters demonstrated that metformin was a significant factor in both final models (Figure 6j, 6k; Supplemental Tables 6 and 7). These data suggested that after adjusting confounders, use of metformin was independently associated with lower raw and indexed ascending aortic diameters, suggesting metformin's potential of delaying aortic dilation and TAA development.

Discussion

In this study, a 3D rhythmically stretching microphysiological model was developed and modified to recapitulate the key biological and biomechanical features of TAA. On the individualized models, we observed that metformin partially reversed phenotypic switching and mitochondrial dysfunction and blocked aortic dilation, which were supported by the murine TAA model and our institutional data. Taken together, we propose the application of a dynamic 3D microenvironment for *in vitro* drug testing for TAA, and the potential of metformin to control TAA progression.

Beyond the traditional static 2D cell culture, microphysiological models are a high-content *in vitro* platform designed to reflect the key biological and biomechanical environment of cells residing in organs.[11,88-90] Numerous biomimetic devices have been developed to promote drug screening and physiological investigation. Huh et al described a 2D co-culture microsystem emulating lung alveoli for nanotoxicology studies[91] Similarly, using a 2D aortic smooth muscle-on-a-chip system, our previous work revealed that mitochondrial dynamics was involved in TAA caused by NOTCH1 insufficiency.[77] Recently, 3D models integrating engineered extracellular matrix or organoids were identified to be more physiologically relevant, with enhanced intercellular mechanotransduction and altered cellular metabolism similar to the native tissues.[16,92] In order to achieve *in vitro* emulation of the aortic medial layer, we designed the current microphysiological model that recapitulated the expressions of many contractile/synthetic phenotypic markers, matrix deposition and remodeling-related genes, and TAA-related pathway genes in thoracic aortic tissues. Particularly, the on-model HAoSMCs exhibited a physiological, contractile phenotype, a reversed state of synthetic phenotype commonly observed in TAA tissues and cells cultured under 2D static condition.[31] These results suggest that cells on the models are in a quasi-physiological state and may presumably have more accurate responses to biological stimuli such as medications.

In addition to these phenotypic imbalances, mitochondrial dysfunction has recently been reported in TAA tissues, characterized by impaired mitochondrial respiration and decreased expressions of oxidative phosphorylation genes.[33,35,76,93] Since the HAoSMCs in the

ascending aortic diameters (marked green). Age, male sex, hypertension, and aortic regurgitation were also significant risk factors for ascending aortic diameter. Values are presented in means ± standard deviations for all panels. ns, P > 0.05; *, P < 0.05; **, P < 0.01; ***, P < 0.001.

aortic medial layer are constantly bearing loads, mitochondrial dysfunction may result in insufficient ATP production for contractile activities. Consistently, we observed that under 3D dynamic culture, the diseased HAoSMCs exhibited lower mitochondrial membrane potential, higher superoxide accumulation, and abnormal oxidative phosphorylation compared with nondiseased cells. These metabolic differences were not evident between the 2D-cultured HAoSMCs, further supporting the superiority of this microphysiological model in reflecting the pathophysiology of TAA.

According to the current clinical guidelines, there is no pathogenesis-targeting medication for controlling TAA.[87] To evaluate the practicality of the microphysiological model in screening drugs and providing preclinical evidence for future trials, we tested 3 drugs on models using physiological concentrations based on the pharmacokinetic studies.

When we determine whether a drug is potentially "beneficial" or "harmful", we take into consideration the overall changes of gene expression before and after drug treatment. In the individualized models of 8 TAA patients, the expressions of many TAA-related genes were not remarkably changed after 7 days of drug treatment, while metformin significantly upregulated the expressions of ACTA2, TIMP1 and TGFB1. ACTA2 and TGFB1 were two genes significantly downregulated in TAA tissues compared with control tissues (Figure 2i), and metformin rescued their expressions. For TIMP1, previous studies showed that knock-in of TIMP1 is associated with halted aortic dilation.[79,81,94] Losartan exhibited minimal rescue of the overall pathological changes, suggesting that apart from its antihypertensive effect, this drug impacted little on the HAoSMCs derived from nonhereditary TAA tissues[49,95] Overactivation of TGF-β pathway has been extensively reported in Marfan syndrome mice with FBN1 mutation.[5,96] However, a paradoxical phenomenon was noticed that loss-of-function mutations in multiple TGF-β pathway genes coexisted with increases in the downstream TGF-β signaling pathway.[97] For TAAs of other etiologies, it should be noted that TGFB1 and MAPK1 are not uniformly upregulated in sporadic or bicuspid aortic valve-related TAA as in Marfan syndrome TAA.[98-100] In contrast, previous studies reported downregulation of TGFB1 and MAPK1, rather than upregulation, in bicuspid aortic valve-related TAA.[74,101,102] In our study, the expressions of TGFB1 and MAPK1 were lower in TAA tissues than control. After a higher ciprofloxacin treatment, the expressions of ACTA2, ELN and MFAP4 were downregulated to a much lower level than normal. Such strong inhibition of contractile phenotype and matrix synthesis validated the harmful effect of 100 μM ciprofloxacin on HAoSMCs. The isolated upregulation of TGFB1 was not as conclusive and presumably inadequate to compensate for the phenotypic inhibition. The drug selection results were consistent with recent clinical studies warning clinicians of fluoroquinolone-related aortic complications.[45]

Metformin is a first-line antidiabetic agent that shows potential effects on cancer and vascular diseases.[41,49,55,84,103,104] As a mitochondrial respiratory complex I inhibitor, the supra-pharmacological use of metformin exhibits its anticancer potential by suppressing cancer cell proliferation and metabolism.[84,105,106] However, it should be noted that metformin's effect on human cells is dose-dependent: while the supra-pharmacological metformin (500-1,000 μM) concentrations used in many studies inhibit mitochondrial respiration, pharmacological metformin concentration (<100 μM) improves such activity, possibly through the AMPK signaling.[107,108] One recent study also revealed the mechanism of low-dose metformin in activating lysosomal AMPK pathway.[109] In this study, we found on the models that metformin, when administered at a physiological concentration in the mammalian peripheral blood (20 μM),[50] the expressions of ACTA2, TAGLN, TIMP1, and TGFB1 were changed. The balance between contractile and synthetic phenotypes was restored, and dysregulations in mitochondrial membrane potential, superoxide accumulation, OCR, and expressions of mitochondrial genes were partially recovered after metformin treatment. Moreover, the *in vivo* validation experiments also indicated the beneficial effect of metformin on TAA. Supraphysiological doses of metformin (200 μM and 1mM) downregulated the expressions of contractile markers (ACTA2 and TAGLN), TGFB1 and TFAM, and upregulated OPN (Supplemental Figure 14), which suggested a pro-TAA phenotype.

The diabetic population was reported to have a lower risk of developing abdominal aortic aneurysm, but such relationship was not sufficiently confirmed in the context of TAA.[42,49,110] Previous studies have shown that TAA has distinct pathogenic, biomechanical, and histologic characteristics from abdominal aortic aneurysm.[8,111,112] While abdominal aortic aneurysm is largely associated with hyperlipidemia and hypertension, as modeled by the ApoE$^{-/-}$ + angiotensin II mice,[10,80] TAA is a more complicated, multifactorial disease not evidently associated with diabetes. From an embryonic perspective, the aortic smooth muscle cells in the ascending thoracic aorta differentiate from progenitor cells in the secondary heart field and neural crest regions, while the cells in the abdominal aorta are from the mesoderm.[113] Previous studies have shown the impact of lineage-specificity on aortic pathologies,[28,114] which could also be causative.

It should be noted that the BAPN-based rodent model could not fully mimic the pathology of TAA in human, and our patient-derived microphysiological model may serve as an auxiliary tool for drug testing. In the BAPN-based mouse TAA models of this study, the most significant dilation occurs in the aortic arch

(1.18 mm *vs.* 2.25 mm, ANOVA, P<0.01), followed by the ascending aorta (1.10 mm *vs.* 1.63 mm, ANOVA, P<0.01). Descending aorta did not significantly dilate after BAPN treatment (0.87 mm *vs.* 0.91 mm, ANOVA, P=0.7560). Metformin's specificity could be attributed to the fact that the aortic arch is the most affected region in this animal model. There has been no study investigating the regional vulnerability of the thoracic aorta to BAPN-induced dilation. There is a possibility that BAPN could be lineage-specific and affect the secondary heart field-derived cells to a lesser extent. Future experiments are warranted to validate this hypothesis.

Altogether, we have shown the potential benefit of metformin in treating TAA at the levels of the microphysiological models, mouse experiments and human clinical investigation. The first advantage of our device is the capability of recapitulating phenotypic switching and mitochondrial dysfunction in TAA tissues. Second, natural hydrogel-forming proteins such as collage type I often lack consistent properties and contain impurities, resulting in high batch-to-batch variation, while the synthetic hydrogel, GelMA, has the advantage of reproducible, well-defined and tunable physicochemical properties.[19] Besides, the fast and on-demand crosslinking process of GelMA hydrogel minimizes cell sedimentation and improves dispersibility.[46] In addition, our patient-derived models showed different yet generally convergent responses to several drugs, suggesting the common features in a heterogenous study population. Our study has taken a step forward in microphysiological model-based translational research for aortic diseases. These promising results may encourage more drugs to be tested on the human-relevant models, which may hopefully improve the clinical translation of new drugs for TAA patients.

There are several limitations in this study. First, although this microphysiological model recapitulated several key features of HAoSMCs in the native ascending aorta, the *in vivo* biological and biomechanical microenvironment is much more complicated. In addition to rhythmic strain, HAoSMCs in tunica media are subject to hydrostatic pressure and shear stress.[4,36,115] Nevertheless, our results demonstrated the predominant role of rhythmic strain in controlling HAoSMC status and behavior. Second, our 3D model is not an ideal platform for protein quantification assays such as Western-blotting due to disturbance from the protein-rich, GelMA-based hydrogel. An effective protein extracting protocol should broaden the application of this device in studying the mechanisms of TAA. Finally, in our clinical data, metformin was administered to diabetic patients only because of the on-label usage of the drug. Regarding concerns about the side effects, several randomized trials have shown the safety of metformin for non-diabetic patients.[116,117] Further retrospective or prospective investigations are warranted to compare TAA progression in patients with and without metformin therapy.

Contributors

Conceptualization, K.Z., C.W., and W.Z.; Methodology, K.Z., W.Z., W.M., J.Z., K.X., S.Y., M.A., S.Z., S.L., H.H., Y.T., N.C., X.S., J.L., and H.L.; Investigation, W.M., J.Z., K.X., S.Y., M.A., Y.M., S.Z., B.X., X.Z., S.L., S.Z., S.L., Z.X., and W.Z.; Formal Analysis, W.M., J.Z., K.Z., and W.Z.; Writing – Original Draft, W.M., J.Z., Y.S.Z., K. Z., and W.Z.; Writing – Review & Editing, W.M., J.Z., Y.S.Z., K.Z., C.W., and W.Z.; Funding Acquisition, K. Z., C.W., and W.Z.; Data Verification and Supervision, K.Z., C.W., and W.Z. All authors read and approved the final version of the manuscript. K.Z., C.W., and W.Z. have accessed and verified the data, and K.Z., C.W., and W.Z. were responsible for the decision to submit the manuscript.

Data Sharing Statement

All the data supporting the findings of this study are available within the article and its Supplemental Information files or from the corresponding author upon reasonable request.

Declaration of interests

None declared.

Acknowledgments

The authors thank Yulin Liang, MS, North University of China, for his support in finite element analysis. This work was supported by grants from National Key R&D Program of China (2018YFC1005002), National Natural Science Foundation of China (82070482, 81771971, 81772007, 51927805, and 21734003), the Science and Technology Commission of Shanghai Municipality (20ZR1411700, 18ZR1407000, 17JC1400200, and 20YF1406900), Shanghai Municipal Science and Technology Major Project (2017SHZDZX01), and Shanghai Municipal Education Commission (Innovation Program 2017-01-07-00-07-E00027). Y.S.Z. was not supported by any of these funds; instead, the Brigham Research Institute is acknowledged.

Supplementary materials

Supplementary material associated with this article can be found in the online version at doi:10.1016/j.ebiom.2022.104080.

References

1 Hiratzka LF, Bakris GL, Beckman JA, et al. 2010 ACCF/AHA/AATS/ACR/ASA/SCA/SCAI/SIR/STS/SVM guidelines for the diagnosis and management of patients with Thoracic Aortic Disease: a report of the American College of Cardiology Foundation/American Heart Association Task Force on Practice Guidelines, American Association for Thoracic Surgery, American College of Radiology, American Stroke Association, Society of Cardiovascular Anesthesiologists, Society for Cardiovascular Angiography and

Interventions, Society of Interventional Radiology, Society of Thoracic Surgeons, and Society for Vascular Medicine. *Circulation*. 2010;121(13):e266–e369.
2 Olsson C, Thelin S, Stahle E, Ekbom A, Granath F. Thoracic aortic aneurysm and dissection: increasing prevalence and improved outcomes reported in a nationwide population-based study of more than 14,000 cases from 1987 to 2002. *Circulation*. 2006;114 (24):2611–2618.
3 Verstraeten A, Luyckx I, Loeys B. Aetiology and management of hereditary aortopathy. *Nat Rev Cardiol*. 2017;14(4):197–208.
4 Humphrey JD, Tellides G. Central artery stiffness and thoracic aortopathy. *Am J Physiol Heart Circ Physiol*. 2019;316(1):H169–HH82.
5 Isselbacher EM, Lino Cardenas CL, Lindsay ME. Hereditary influence in thoracic aortic aneurysm and dissection. *Circulation*. 2016;133(24):2516–2528.
6 Pannu H, Avidan N, Tran-Fadulu V, Milewicz DM. Genetic basis of thoracic aortic aneurysms and dissections: potential relevance to abdominal aortic aneurysms. *Ann NY Acad Sci*. 2006;1085:242–255.
7 Pinard A, Jones GT, Milewicz DM. Genetics of Thoracic and Abdominal Aortic Diseases. *Circ Res*. 2019;124(4):588–606.
8 Braverman AC. Medical management of thoracic aortic aneurysm disease. *J Thorac Cardiovasc Surg*. 2013;145(3 Suppl). S2-6.
9 Milewicz DM, Ramirez F. Therapies for Thoracic Aortic Aneurysms and Acute Aortic Dissections. *Arterioscler Thromb Vasc Biol*. 2019;39(2):126–136.
10 Lindeman JH, Matsumura JS. Pharmacologic management of aneurysms. *Circ Res*. 2019;124(4):631–646.
11 Yesil-Celiktas O, Hassan S, Miri AK, et al. Mimicking human pathophysiology in organ-on-chip devices. *Adv Biosyst*. 2018;2(10).
12 Musah S, Mammoto A, Ferrante TC, et al. Mature induced-pluripotent-stem-cell-derived human podocytes reconstitute kidney glomerular-capillary-wall function on a chip. *Nat Biomed Eng*. 2017;1.
13 Osaki T, Shin Y, Sivathanu V, Campisi M, Kamm RD. In vitro microfluidic models for neurodegenerative disorders. *Adv Healthc Mater*. 2018;7(2).
14 Zhang YS, Khademhosseini A. Engineering in vitro human tissue models through bio-design and manufacturing. *Bio-Des Manuf*. 2020;3(3):155–159.
15 Ingber DE. Is it time for reviewer 3 to request human organ chip experiments instead of animal validation studies? *Adv Sci (Weinh)*. 2020;7:(22) 2002030.
16 Occhetta P, Mainardi A, Votta E, et al. Hyperphysiological compression of articular cartilage induces an osteoarthritic phenotype in a cartilage-on-a-chip model. *Nat Biomed Eng*. 2019;3(7):545–557.
17 Kilic O, Yoon A, Shah SR, et al. A microphysiological model of the bronchial airways reveals the interplay of mechanical and biochemical signals in bronchospasm. *Nat Biomed Eng*. 2019;3(7):532–544.
18 Ribas J, Zhang YS, Pitrez PR, et al. Biomechanical strain exacerbates inflammation on a progeria-on-a-chip model. *Small*. 2017;13(15).
19 Loessner D, Meinert C, Kaemmerer E, et al. Functionalization, preparation and use of cell-laden gelatin methacryloyl-based hydrogels as modular tissue culture platforms. *Nat Protoc*. 2016;11 (4):727–746.
20 Cao X, Ashfaq R, Cheng F, et al. A Tumor-on-a-Chip System with Bioprinted Blood and Lymphatic Vessel Pair. 2019; 29(31): 1807173.
21 Gong J, Schuurmans CCL, AMv Genderen, et al. Complexation-induced resolution enhancement of 3D-printed hydrogel constructs. *Nat Commun*. 2020;11(1):1267.
22 Liu T, Liu Q, Anaya I, et al. Investigating lymphangiogenesis in a sacrificially bioprinted volumetric model of breast tumor tissue. *Methods*. 2020.
23 Zhao X, Liu Y, Shao C, et al. Photoresponsive delivery microcarriers for tissue defects repair. *Adv Sci (Weinh)*. 2019;6:(20) 1901280.
24 Cai L, Chen G, Wang Y, Zhao C, Shang L, Zhao Y. Boston ivy-inspired disc-like adhesive microparticles for drug delivery. *Research (Wash D C)*. 2021;2021: 9895674.
25 Sun L, Chen Z, Xu D, Zhao Y. Electroconductive and anisotropic structural color hydrogels for visual heart-on-a-chip construction. *Adv Sci (Weinh)*. 2022 e2105777.
26 Chen YC, Lin RZ, Qi H, et al. Functional human vascular network generated in photocrosslinkable gelatin methacrylate hydrogels. *Adv Funct Mater*. 2012;22(10):2027–2039.
27 Pedroza AJ, Tashima Y, Shad R, et al. Single-cell transcriptomic profiling of vascular smooth muscle cell phenotype modulation in Marfan syndrome aortic aneurysm. *Arterioscler Thromb Vasc Biol*. 2020;40(9):2195–2211.
28 MacFarlane EG, Parker SJ, Shin JY, et al. Lineage-specific events underlie aortic root aneurysm pathogenesis in Loeys-Dietz syndrome. *J Clin Invest*. 2019;129(2):659–675.
29 Quintana RA, Taylor WR. Cellular mechanisms of aortic aneurysm formation. *Circ Res*. 2019;124(4):607–618.
30 Yang K, Ren J, Li X, et al. Prevention of aortic dissection and aneurysm via an ALDH2-mediated switch in vascular smooth muscle cell phenotype. *Eur Heart J*. 2020;41(26):2442–2453.
31 Hulsmans M, Nahrendorf M. Proliferative, degradative smooth muscle cells promote aortic disease. *J Clin Invest*. 2020;130 (3):1096–1098.
32 Petsophonsakul P, Furmanik M, Forsythe R, et al. Role of vascular smooth muscle cell phenotypic switching and calcification in aortic aneurysm formation. *Arterioscler Thromb Vasc Biol*. 2019;39 (7):1351–1368.
33 Oller J, Gabande-Rodriguez E, Ruiz-Rodriguez MJ, et al. Extracellular tuning of mitochondrial respiration leads to aortic aneurysm. *Circulation*. 2021.
34 Gutierrez PS, Piubelli MLM, Naal KG, Dias RR, Borges LF. Mitochondria in aneurysms and dissections of the human ascending aorta. *Cardiovasc Pathol*. 2020;47: 107207.
35 Li Y, Ren P, Dawson A, et al. Single-cell transcriptome analysis reveals dynamic cell populations and differential gene expression patterns in control and aneurysmal human aortic tissue. *Circulation*. 2020;142(14):1374–1388.
36 Dan P, Velot E, Decot V, Menu P. The role of mechanical stimuli in the vascular differentiation of mesenchymal stem cells. *J Cell Sci*. 2015;128(14):2415–2422.
37 Mantella LE, Quan A, Verma S. Variability in vascular smooth muscle cell stretch-induced responses in 2D culture. *Vascular cell*. 2015;7:7.
38 Kinnear C, Chang WY, Khattak S, et al. Modeling and rescue of the vascular phenotype of Williams-Beuren syndrome in patient induced pluripotent stem cells. *Stem Cells Transl Med*. 2013;2(1):2–15.
39 Paul RS, Antonino C, Brian PN, Christian TP, Melinda AS. Cyclic stretch induces vascular smooth muscle cell alignment via NO signaling. *Am J Physiol Heart Circ Physiol*. 2002;283(5). H1907-H14.
40 Yi HG, Jeong YH, Kim Y, et al. A bioprinted human-glioblastoma-on-a-chip for the identification of patient-specific responses to chemoradiotherapy. *Nat Biomed Eng*. 2019;3(7):509–519.
41 Yu X, Jiang D, Wang J, et al. Metformin prescription and aortic aneurysm: systematic review and meta-analysis. *Heart*. 2019;105 (17):1351–1357.
42 Itoga NK, Rothenberg KA, Suarez P, et al. Metformin prescription status and abdominal aortic aneurysm disease progression in the U.S. veteran population. *J Vasc Surg*. 2019;69(3). 710-6 e3.
43 Bossone E, Eagle KA. Epidemiology and management of aortic disease: aortic aneurysms and acute aortic syndromes. *Nat Rev Cardiol*. 2020.
44 Jennifer PH, Daniel PJ, Tammy MH, et al. Losartan, an AT1 antagonist, prevents aortic aneurysm in a mouse model of Marfan syndrome. *Science*. 2006;312(5770):117–121.
45 LeMaire SA, Zhang L, Luo W, et al. Effect of ciprofloxacin on susceptibility to aortic dissection and rupture in mice. *JAMA Surg*. 2018;153:(9) e181804.
46 Chen N, Zhu K, Zhang YS, et al. Hydrogel Bioink with multilayered interfaces improves dispersibility of encapsulated cells in extrusion bioprinting. *ACS Appl Mater Interfaces*. 2019;11 (34):30585–30595.
47 Park SE, Georgescu A, Oh JM, Kwon KW, Huh D. Polydopamine-based interfacial engineering of extracellular matrix hydrogels for the construction and long-term maintenance of living three-dimensional tissues. *ACS Appl Mater Interfaces*. 2019;11(27):23919–23925.
48 Wang Z, Volinsky AA, Gallant ND. Crosslinking effect on polydimethylsiloxane elastic modulus measured by custom-built compression instrument. *J Appl Polym Sci*. 2014;131(22).
49 Fujimura N, Xiong J, Kettler EB, et al. Metformin treatment status and abdominal aortic aneurysm disease progression. *J Vasc Surg*. 2016;64(1). 46-54 e8.
50 Wilcock C, Bailey CJ. Accumulation of metformin by tissues of the normal and diabetic mouse. *Xenobiotica*. 1994;24(1):49–57.
51 Ohtawa M, Takayama F, Saitoh K, Yoshinaga T, Nakashima M. Pharmacokinetics and biochemical efficacy after single and multiple oral administration of losartan, an orally active nonpeptide angiotensin II receptor antagonist, in humans. *Br J Clin Pharmacol*. 1993;35(3):290–297.

52 Sica DA, Gehr TW, Ghosh S. Clinical pharmacokinetics of losartan. *Clin Pharmacokinet*. 2005;44(8):797–814.
53 Brunner M, Stabeta H, Moller JG, et al. Target site concentrations of ciprofloxacin after single intravenous and oral doses. *Antimicrob Agents Chemother*. 2002;46(12):3724–3730.
54 Lode H, Borner K, Koeppe P. Pharmacodynamics of fluoroquinolones. *Clin Infect Dis*. 1998;27(1):33–39.
55 Foretz M, Guigas B, Bertrand L, Pollak M, Viollet B. Metformin: from mechanisms of action to therapies. *Cell Metab*. 2014;20(6):953–966.
56 Kardon DE, Borczuk AC, Factor SM. Mechanism of pericardial expansion with cardiac enlargement. *Cardiovasc Pathol*. 2000;9(1):9–15.
57 Bharath LP, Agrawal M, McCambridge G, et al. Metformin enhances autophagy and normalizes mitochondrial function to alleviate aging-associated inflammation. *Cell Metab*. 2020;32(1). 44-55 e6.
58 Bell V, Mitchell WA, Sigurethsson S, et al. Longitudinal and circumferential strain of the proximal aorta. *J Am Heart Assoc*. 2014;3:(6) e001536.
59 Longobardo L, Carerj ML, Pizzino G, et al. Impairment of elastic properties of the aorta in bicuspid aortic valve: relationship between biomolecular and aortic strain patterns. *Eur Heart J Cardiovasc Imaging*. 2018;19(8):879–887.
60 Morrison TM, Choi G, Zarins CK, Taylor CA. Circumferential and longitudinal cyclic strain of the human thoracic aorta: age-related changes. *J Vasc Surg*. 2009;49(4):1029–1036.
61 Akazawa Y, Motoki N, Tada A, et al. Decreased aortic elasticity in children with marfan syndrome or loeys-dietz syndrome. *Circ J*. 2016;80(11):2369–2375.
62 Guala A, Teixido-Tura G, Rodriguez-Palomares J, et al. Proximal aorta longitudinal strain predicts aortic root dilation rate and aortic events in Marfan syndrome. *Eur Heart J*. 2019;40(25):2047–2055.
63 Pasta S, Agnese V, Di Giuseppe M, et al. In vivo strain analysis of dilated ascending thoracic aorta by ECG-Gated CT angiographic imaging. *Ann Biomed Eng*. 2017;45(12):2911–2920.
64 Granata A, Serrano F, Bernard WG, et al. An iPSC-derived vascular model of Marfan syndrome identifies key mediators of smooth muscle cell death. *Nat Genet*. 2017;49(1):97–109.
65 Jager MA, De La Torre C, Arnold C, et al. Assembly of vascular smooth muscle cells in 3D aggregates provokes cellular quiescence. *Exp Cell Res*. 2020;388:(1) 111782.
66 Ganesan MK, Finsterwalder R, Leb H, et al. Three-dimensional coculture model to analyze the cross talk between endothelial and smooth muscle cells. *Tissue Eng Part C Methods*. 2017;23(1):38–49.
67 Chapman GB, Durante W, Hellums JD, Schafer AI. Physiological cyclic stretch causes cell cycle arrest in cultured vascular smooth muscle cells. *Am J Physiol Heart Circ Physiol*. 2000;278(3). H748-54.
68 Isenberg BC, Tranquillo RT. Long-term cyclic distention enhances the mechanical properties of collagen-based media-equivalents. *Ann Biomed Eng*. 2003;31(8):937–949.
69 Ramaswamy AK, Sides RE, Cunnane EM, et al. Adipose-derived stromal cell secreted factors induce the elastogenesis cascade within 3D aortic smooth muscle cell constructs. *Matrix Biol Plus*. 2019;4: 100014.
70 Ziganshin BA, Bailey AE, Coons C, et al. Routine genetic testing for thoracic aortic aneurysm and dissection in a clinical setting. *Ann Thorac Surg*. 2015;100(5):1604–1611.
71 Golledge J, Muller J, Shephard N, et al. Association between osteopontin and human abdominal aortic aneurysm. *Arterioscler Thromb Vasc Biol*. 2007;27(3):655–660.
72 Yin X, Wanga S, Fellows AL, et al. Glycoproteomic analysis of the aortic extracellular matrix in marfan patients. *Arterioscler Thromb Vasc Biol*. 2019;39(9):1859–1873.
73 Angelov SN, Hu JH, Wei H, Airhart N, Shi M, Dichek DA. TGF-beta (transforming growth factor-beta) signaling protects the thoracic and abdominal aorta from angiotensin ii-induced pathology by distinct mechanisms. *Arterioscler Thromb Vasc Biol*. 2017;37(11):2102–2113.
74 Balint B, Yin H, Nong Z, et al. Seno-destructive smooth muscle cells in the ascending aorta of patients with bicuspid aortic valve disease. *EBioMedicine*. 2019;43:54–66.
75 Lindholt JS, Madsen M, Kirketerp-Moller KL, et al. High plasma microfibrillar-associated protein 4 is associated with reduced surgical repair in abdominal aortic aneurysms. *J Vasc Surg*. 2020;71(6):1921–1929.
76 Yu E, Foote K, Bennett M. Mitochondrial function in thoracic aortic aneurysms. *Cardiovasc Res*. 2018;114(13):1696–1698.
77 Abudupataer M, Zhu S, Yan S, et al. Aorta smooth muscle-on-a-chip reveals impaired mitochondrial dynamics as a therapeutic target for aortic aneurysm in bicuspid aortic valve disease. *Elife*. 2021;10.
78 Guo DC, Pannu H, Tran-Fadulu V, et al. Mutations in smooth muscle alpha-actin (ACTA2) lead to thoracic aortic aneurysms and dissections. *Nat Genet*. 2007;39(12):1488–1493.
79 Allaire E, Forough R, Clowes M, Starcher B, Clowes AW. Local overexpression of TIMP-1 prevents aortic aneurysm degeneration and rupture in a rat model. *J Clin Invest*. 1998;102(7):1413–1420.
80 Bruemmer D, Collins AR, Noh G, et al. Angiotensin II-accelerated atherosclerosis and aneurysm formation is attenuated in osteopontin-deficient mice. *J Clin Invest*. 2003;112(9):1318–1331.
81 Xiong W, Meisinger T, Knispel R, Worth JM, Baxter BT. MMP-2 regulates Erk1/2 phosphorylation and aortic dilatation in Marfan syndrome. *Circ Res*. 2012;110(12):e92–e101.
82 Pasternak B, Inghammar M, Svanstrom H. Fluoroquinolone use and risk of aortic aneurysm and dissection: nationwide cohort study. *BMJ*. 2018;360:k678.
83 Lee J, Yesilkanal AE, Wynne JP, et al. Effective breast cancer combination therapy targeting BACH1 and mitochondrial metabolism. *Nature*. 2019;568(7751):254–258.
84 Vancura A, Bu P, Bhagwat M, Zeng J, Vancurova I. Metformin as an anticancer agent. *Trends Pharmacol Sci*. 2018;39(10):867–878.
85 Watson A, Nong Z, Yin H, et al. Nicotinamide phosphoribosyltransferase in smooth muscle cells maintains genome integrity, resists aortic medial degeneration, and is suppressed in human thoracic aortic aneurysm disease. *Circ Res*. 2017;120(12):1889–1902.
86 Zou Y, Wang A, Huang L, et al. Illuminating NAD(+) metabolism in live cells and in vivo using a genetically encoded fluorescent sensor. *Dev Cell*. 2020;53(2). 240-52 e7.
87 Borger MA, Fedak PWM, Stephens EH, et al. The American association for thoracic surgery consensus guidelines on bicuspid aortic valve-related aortopathy: Full online-only version. *J Thorac Cardiovasc Surg*. 2018;156(2):e41–e74.
88 Nie J, Gao Q, Wang Y, et al. Vessel-on-a-chip with Hydrogel-based Microfluidics. *Small*. 2018;14:(45) e1802368.
89 Chen P, Zhang X, Ding R, et al. Patient-derived organoids can guide personalized-therapies for patients with advanced breast cancer. *Adv Sci (Weinh)*. 2021;8:(22) e2101176.
90 Li Z, Xu H, Gong Y, et al. Patient-derived upper tract urothelial carcinoma organoids as a platform for drug screening. *Adv Sci (Weinh)*. 2021 e2103999.
91 Dongeun H, Benjamin DM, Akiko M, Martín M-Z, Hong YH, Donald EI. Reconstituting organ-level lung functions on a chip. *Science*. 2010;328(5986):1662–1668.
92 Gjorevski N, Nikolaev M, Brown TE, et al. Tissue geometry drives deterministic organoid patterning. *Science*. 2022;375(6576):eaaw9021.
93 Hawk MA, Gorsuch CL, Fagan P, et al. RIPK1-mediated induction of mitophagy compromises the viability of extracellular-matrix-detached cells. *Nat Cell Biol*. 2018;20(3):272–284.
94 LeMaire SA, Wang X, Wilks JA, et al. Matrix metalloproteinases in ascending aortic aneurysms: bicuspid versus trileaflet aortic valves. *J Surg Res*. 2005;123(1):40–48.
95 Habashi JP, Judge DP, Holm TM, et al. Losartan, an AT1 antagonist, prevents aortic aneurysm in a mouse model of Marfan syndrome. *Science*. 2006;312(5770):117–121.
96 Wu Y, Sun H, Wang J, et al. Marfan syndrome: whole-exome sequencing reveals de novo mutations, second gene and genotype-phenotype correlations in the Chinese population. *Biosci Rep*. 2020;40(12).
97 Akhurst RJ. The paradoxical TGF-beta vasculopathies. *Nat Genet*. 2012;44(8):838–839.
98 Jiao J, Xiong W, Wang L, et al. Differentiation defect in neural crest-derived smooth muscle cells in patients with aortopathy associated with bicuspid aortic valves. *EBioMedicine*. 2016;10:282–290.
99 Heng E, Stone JR, Kim JB, Lee H, MacGillivray TE, Sundt TM. Comparative histology of aortic dilatation associated with bileaflet versus trileaflet aortic valves. *Ann Thorac Surg*. 2015;100(6):2095–2101. discussion 101.
100 Phillippi JA, Green BR, Eskay MA, et al. Mechanism of aortic medial matrix remodeling is distinct in patients with bicuspid aortic valve. *J Thorac Cardiovasc Surg*. 2014;147(3):1056–1064.
101 Paloschi V, Gadin JR, Khan S, et al. Aneurysm development in patients with a bicuspid aortic valve is not associated with transforming growth factor-beta activation. *Arterioscler Thromb Vasc Biol*. 2015;35(4):973–980.

102 Zhang L, Zhou J, Jing Z, et al. Glucocorticoids regulate the vascular remodeling of aortic dissection via the p38 MAPK-HSP27 pathway mediated by soluble TNF-RII. *EBioMedicine*. 2018;27:247–257.
103 Soukas AA, Hao H, Wu L. Metformin as Anti-aging therapy: is it for everyone? *Trends Endocrinol Metab*. 2019;30(10):745–755.
104 Vasan K, Werner M, Chandel NS. Mitochondrial metabolism as a target for cancer therapy. *Cell Metab*. 2020;32(3):341–352.
105 Wheaton WW, Weinberg SE, Hamanaka RB, et al. Metformin inhibits mitochondrial complex I of cancer cells to reduce tumorigenesis. *Elife*. 2014;3:e02242.
106 Howell JJ, Hellberg K, Turner M, et al. Metformin inhibits hepatic mTORC1 signaling via dose-dependent mechanisms involving AMPK and the TSC complex. *Cell Metab*. 2017;25(2):463–471.
107 Wang Y, An H, Liu T, et al. Metformin improves mitochondrial respiratory activity through activation of AMPK. *Cell Rep*. 2019;29 (6). 1511-23 e5.
108 Alshawi A, Agius L. Low metformin causes a more oxidized mitochondrial NADH/NAD redox state in hepatocytes and inhibits gluconeogenesis by a redox-independent mechanism. *J Biol Chem*. 2019;294(8):2839–2853.
109 Ma T, Tian X, Zhang B, et al. Low-dose metformin targets the lysosomal AMPK pathway through PEN2. *Nature*. 2022;603 (7899):159–165.
110 Sutton SS, Magagnoli J, Cummings TH, Hardin JW. Association between metformin and abdominal aortic aneurysm in diabetic and non-diabetic US veterans. *J Investig Med*. 2020;68(5):1015–1018.
111 Cebull HL, Rayz VL, Goergen CJ. Recent advances in biomechanical characterization of thoracic aortic aneurysms. *Front Cardiovasc Med*. 2020;7:75.
112 Dingemans KP, Teeling P, Lagendijk JH, Becker AE. Extracellular matrix of the human aortic media: an ultrastructural histochemical and immunohistochemical study of the adult aortic media. *Anat Rec*. 2000;258(1):1–14.
113 Gadson Jr. PF, Dalton ML, Patterson E, et al. Differential response of mesoderm- and neural crest-derived smooth muscle to TGF-beta1: regulation of c-myb and alpha1 (I) procollagen genes. *Exp Cell Res*. 1997;230(2):169–180.
114 Gong J, Zhou D, Jiang L, et al. In vitro lineage-specific differentiation of vascular smooth muscle cells in response to SMAD3 deficiency: implications for SMAD3-related thoracic aortic aneurysm. *Arterioscler Thromb Vasc Biol*. 2020;40(7):1651–1663.
115 Sugita S, Kato M, Wataru F, Nakamura M. Three-dimensional analysis of the thoracic aorta microscopic deformation during intraluminal pressurization. *Biomech Model Mechanobiol*. 2020;19(1):147–157.
116 El Messaoudi S, Nederlof R, Zuurbier CJ, et al. Effect of metformin pretreatment on myocardial injury during coronary artery bypass surgery in patients without diabetes (MetCAB): a double-blind, randomised controlled trial. *Lancet Diabetes Endocrinol*. 2015;3 (8):615–623.
117 Preiss D, Lloyd SM, Ford I, et al. Metformin for non-diabetic patients with coronary heart disease (the CAMERA study): a randomised controlled trial. *Lancet Diabetes Endocrinol*. 2014;2(2):116–124.